Aalto University
School of Chemical
Technology

School of Chemical Technology
Degree Programme of Materials Science and Engineering

Luca Reali

MODELLING AND ANALYSIS OF BEHAVIOUR OF BIOMEDICAL SCAFFOLDS

Final Project (15 cr) submitted for inspection, Espoo, 18^{th} May, 2015.

Supervisor Professor Michael Gasik

Instructor Ph.D. Yevgen Bilotsky

Aalto University
School of Chemical
Technology

Aalto University, P.O. BOX 11000, 00076 AALTO
www.aalto.fi
Abstract of Final Project

Author	Luca Reali
Title of final project	MODELLING AND ANALYSIS OF BEHAVIOUR OF BIOMEDICAL SCAFFOLDS
Department	Materials Science and Engineering
Professorship	Material Processing **Code of professorship** MT-77
Thesis supervisor	Professor Michael Gasik
Thesis advisor / Thesis examiner	Ph.D. Yevgen Bilotsky
Date	18.05.2015 **Number of pages** 75 **Language** English

Abstract

Since articular cartilage related diseases are an increasing issue and they are nowadays treated by invasive prosthesis implantations, there is a strong demand for new solutions such as those offered by scaffold engineering. This work deals with the characterization and modelling of polymeric fabrics for cartilage repair. Creep tests data at three different applied forces were successfully modelled both analytically, using viscoelastic models, and by finite element analysis which embraced the theory of poroelasticity. A linear correlation between the viscoelastic parameters brought to the definition of a time dependent effective modulus function of the applied force and based on a set of four material parameters, whereas a finite element parametric analysis lead to the estimation of the matrix intrinsic permeability. Finally the behaviour of the material in both creep and dynamic loading configurations was studied using the finite element method, starting from the results of the previous characterization for the setup of the simulations. The attention was mainly focused on the fluid related quantities pore pressure and velocity field because of their importance in transferring mechanical stimuli to cells eventually present in a further stage.

Keywords: Viscoelasticity, Poroelasticity, Scaffold Engineering, Finite Elements

"The Universe is written in in the language of mathematics
and its characters are triangles, circles ...
without them it is like wandering in a darkened maze."

G. Galilei

Acknowledgement

This work is the result of the great experience that has been living here in Finland. It has been an honour to study in such an exciting university and to say that, at least a little bit, I now belong to this beautiful country. It was however just the final part of a journey that I had started much earlier.
I want to dedicate it to the many people that meant so much in my life, either if they are here mentioned or not.

To my family, to my mother Anna who not only made me the person I am proud to be but also gave me the desire to learn and taught me never to stop to be curious, to my sister Sarah, who is a treasure I did not deserve and who has always been there for me, to Andrea, who now has the honour to take care of her, to my aunt Vanna, to whom I really owe all of this, I did my best to make good use of a lifetime of work, to my dad Giorgio, without whom I would not be here and to my uncle Vincenzo, who has been a father to me when my father was far away, to whom is not here anymore but, I am sure, would have been proud of their little boy.

Of course a big thanks to my professor in Finland, Michael Gasik, who wanted to have me here in the first place and who has been a guide even too much careful and present, I have never been left on my own during all this. A big thanks also to my professor in Trento, Vigilio Fontanari, whose competence but especially passion for his job has always impressed me.

To Giuliano, for sharing with me efforts and satisfactions in all the pages we turned and in all the rocks we walked past together, and to all my friends at home, you made it hard for me to go away, especially at the very end. You are the spark in my volleyball evenings, the beauty in my mountains, the voice of the songs around a fire, the happiness in endless conversations.
To all my new friends here, because they made it easy to feel at home again, thank you for the coffee ready every morning, for all the dinners and the trips, for giving me so many memories to bring back.

Finally, to my teacher Serena, who planted the first seed of my passion for science, to S. Marco, for teaching me the value of life and to all the people that made me a better person. I will always remember you.

Espoo, 18^{th} May, 2015

Luca

Contents

List of Figures

List of Tables

List of symbols

α	Biot's coefficient	[-]
δ	Loss factor	[-]
δ_{ij}	Kronecker delta	[-]
ϵ	Strain	[-]
$\dot{\epsilon}$	Strain rate	[s^{-1}]
μ	Dynamic viscosity	[Pa·s]
ν	Poisson's ratio	[-]
ρ	Density	[kg·m^{-3}]
σ	Stress	[Pa]
τ	Characteristic time	[s]
ω	Frequency	[s^{-1}]
c_i	Dashpot constant of element i	[Pa·s]
f	Body load	[N·m^{-3}]
i	Imaginary unit	[-]
g	Standard gravity	[m·s^{-2}]
k_i	Spring constant of element i	[Pa]
k	Intrinsic permeability	[m^2]
m	Fluid mass content	[kg·m^{-3}]
n	Porosity	[-]
p	Fluid pressure	[Pa]
q	Discharge velocity	[m·s^{-1}]
u	Displacement	[m]
x_i	Displacement of element i	[m]

B_{ij}	Strain-nodal displacement correlation	[m^{-1}]
D	Compliance	[Pa^{-1}]
E	Elastic modulus	[Pa]
E^*	Dynamic modulus	[Pa]
F	Force	[N]
G	Shear modulus	[Pa]
K	Bulk modulus	[Pa]
K_{ij}	Stiffness matrix	[Pa]
K_{hyd}	Hydraulic conductivity	[$m \cdot s^{-1}$]
L_{ij}	Strain-displacement field correlation	[m^{-1}]
N_{ij}	Shape factors matrix	[-]
V	Volume	[m^3]
T	Tensile stress	[Pa]
U_{ij}	Nodal displacement matrix	[m]
Y_{ij}	Matrix constitutive equation	[Pa]

1 Introduction

1.1 Motivation

Cartilage related diseases are an important issue concerning the health of the human body. The articular cartilage is a peculiar and highly specialized tissue that is subjected to high stresses that result in an unavoidable though surprisingly low wear rate (in a physiological range of load and velocity it was found to be below the limit of measurement [1]). In order to optimize the wear response this tissue does not have the self-healing capability which can be observed in almost all the other tissues. The progressive damage of a joint's surfaces is therefore permanent and can hinder and eventually impede its movement. The fact that the organism cannot heal the cartilage on its own makes this tissue an ideal target for biomedical engineering. The challenge is tackled both by joint replacements, currently the most common solution, and by the design of scaffolds for repair and, ultimately, regenerative medicine. One step further in fact is the possibility of seeding cells inside, moving then toward tissue engineering.
This work is mainly devoted to the understanding of the mechanical behaviour of polymeric scaffolds that could be used to replace only worn parts in the articular surfaces, instead of using prosthesis implants to raplace the whole compartment. The former method would clearly be preferable because much less invasive.
A procedure for the characterization of such devices must be developed to have an idea of the stress and strain that result from physiological solicitations, and also an insight on the fluid flow characteristics, which are the physical stimuli that cells would feel, is desired.

1.2 Objectives

The objectives of this work are therefore firstly the characterization of polymeric scaffolds starting from unconfined compression tests, with the aim of extracting a set of parameters able to describe the mechanical response of the material. In this section the theory of linear viscoelasticity is used. Secondly also finite elements simulations are carried out in order to visualize the evolution of the involved quantities also in their spatial distribution. These simulations used both the results of the viscoelastic fitting and a different approach. In this second case a theory that has been proved to be appropriate is employed. The theory, called poroelasticity, deals with the mechanics of fluid infiltrated porous media. This step forward allows to see the scaffold as a biphasic body where both the displacement of the solid matrix

and the fluid motion within it are solved for. This requires, however, the knowledge of additional parameters for the modelling and this is also one of the points of the simulations. In particular the unknown value is that on the matrix intrinsic permeability and for it an estimation is intended to be obtained. For the sake of the efficiency of the computational analysis the material characterization should be kept as simple as possible avoiding complex models.

1.3 Structure

This work is developed over three main sections.
In the first one a theoretical survey gives the context of the topic. The introduction on the biological aspects of the real tissue lets one understand the complexity of the problem. The viscoelastic mechanical models are then presented, as well as the theory of poroelasticity.
In the second part there is a short presentation of the research methods, which are tests run on a dynamic mechanical analysis (DMA) machine and finite elements method (FEM) simulations.
There is finally the discussion of the results both of the fitting procedure and of the simulations. As it will be shown, the simple theory of linear viscoelasticity is adequate to deal with the single experiment but cannot give parameters dependent only on the material itself. The last part in particular presents some of the quantities that can by obtained in the postprocessing environment.

2 Biomedical survey

2.1 Cartilage

The human body is composed of different tissues, where a tissue is defined as the arrangement of cells and extracellular matrix that together carry out a certain function. The study of tissues is called histology, the study of the connected diseases is called histopathology. There are four basic tissue types: connective, muscle, nervous, epithelial.
Connective tissues are fibrous tissues, such as bone or cartilage. Also blood is sometimes considered a connective tissue. The main role of the connective tissues is to sustain and bind other tissues, this roles being played respectively by bone and tendons and ligaments, fibrous structures which connect muscles to bones or bones to bones.
Muscle tissue is responsible for the active movements of the body. There are three categories of muscle tissue, all capable of contraction: skeletal muscle, attached to the bones and executor of the voluntary movements; smooth muscle, in the inner parts of the body as well as in the tunica media, the central part of the blood vessels, which is the executor of involuntary movements such as the peristalsis; cardiac muscle, the tissue that causes the periodic contraction of the heart, involuntary though striated.
Nervous tissue makes up the central nervous system and the peripheral nervous system. The first is brain and spinal cord, the latter is the network of cranial and spinal nerves to which also the motor neurons belong.
Epithelial tissue has a protective function and it covers all the organ surfaces from the inner lining of the lungs and of the intestine to the skin, covering the whole body.
For each tissue there are specialized cells, usually producers of the similarly highly specialized extracellular matrix. Typically a tissue is also characterized by the cell density and disposition and by the cell to extracellular matrix ratio.

2.1.1 Articular cartilage

Cartilage is a connective tissue present in many parts of the human and animal body. It is divided into three categories: hyaline cartilage, fibrocartilage, elastic cartilage. The hyaline cartilage that covers the surface of a bone forming a joint is called articular cartilage.
The *articular cartilage* is a layer of 1-5 mm of highly specialized connective tissue. Its main functions are to enlarge the contact area in order to lower the applied

stresses and the consequent wear of the surfaces, and to allow the relative motion between the two bones with a friction as low as possible, this again to achieve a wear rate as low as possible. A healthy joint can have a coefficient of dynamic friction surprisingly low of about 0.001 [2]. Just for a quick comparison PTFE sliding on PTFE shows a coefficient of 0.04.

2.1.2 Structure and composition

The main features of the articular cartilage tissue are the very low cell density and the absence, apart from the very external part, of blood vessels, nerves and limphatic vessels. This means that nutriment is supplied to the cells only by diffusion and convection in the liquid phase.
In normal articular cartilage chondrocytes account for less than 10% of the wet tissue's volumetric fraction, collagen accounts for 15% to 22% proteoglycans (PG) for 4% to 7% whereas the remaining 60% to 85% is water, inorganic salts and small amounts of other matrix proteins, glycoproteins and lipids [3]. The structure is made of a matrix of a collagen fibers network, immersed in an interstitial fluid containing proteoglycans, and of cells, which are called chondrocytes. Collagen is the main structural protein, making up about 30% of the whole protein content. It is composed of a triple helix with two identical α_1 chains and another α_2 chain, slightly different. The structure underlying a macroscopic fiber is highly hierarchical and organized from the nano to the micro scale. The single molecule is called tropocollagen and it is approximately 300 nm long. Its three alpha helixes twist and form a right-handed super helix giving the quaternary structure stabilized by hydrogen bonds. The tropocollagen units in turn make up a right-handed super super coil that is called collagen microfibril and that is a very ordered structure. The microfibrils are the building blocks of the collagen fibrils and finally the fibrils united give the collagen fibers. The estimated values from tensile tests are a Young modulus of about 1 GPa and a strength of about 50 MPa. It is worth noting that these are remarkale values, close to the common synthetic polymers and this is not surprising since both of them are carbon based materials. There are over 28 different types of collagen, though 90% of the total is type 1. Type 1 is mostly present in skin, tendons and bone, Type 2 is mainly present in cartilage, type 3 is usually alongside type 1, type 4 forms the basal lamina in the basement membrane.

The structure of the cartilage has peculiar characteristics, that derive from the function needed in that position, as for both the cell density and arrangement and as for the collagen fibers disposition. In the superficial zone, farther from the bone, chondrocytes are oblong and parallel to the surface, in the middle they tend to be

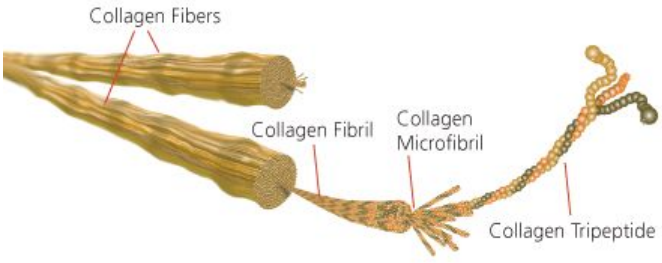

Figure 2.1: The collagen structure

round and random while in the deep zone, closer to the bone, they are perpendicular to the tidemark (that is the layer that separates the true articular cartilage from the deeper, calcified cartilage that is attached to the bone). The same tripartition is visible also as far as the collagen fibers arrangement is concerned. In the superficial zone the fibers are densely packed and parallel to the articular surface, in the middle zone they are less packed and randomly oriented whereas in the deep zone they form bundles radially coming out from the articular-calcified cartilage junction. These bundles cross the tidemark giving a strong interlock between cartilage and bone. The reason for this fiber arrangement can be found thinking about the local stresses that may arise: the surface is subjected to a high contact pressure and the Hertzian theory considers the presence of a tangential stress that needs to be sustained while the radial disposition is the best way to provide as much linkage as possible capable to react in every direction. In the middle zone the fiber density decreases in order to give space for the high amount of water and PG needed for the compressive strength.

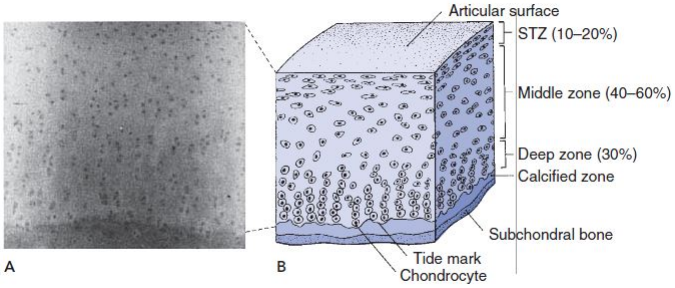

Figure 2.2: Chondrocytes disposition as visible in (A) a micrograph and (B) a schematic representation in a healthy articular cartilage [3].

One may wonder what are the origins of the mechanical characteristics of the cartilage. The first feature in this sense comes from the fact that this tissue is very rich in water since its volumetric amount ranges from about 80% at the surface to about 65% at the deep zone.

An important component to explain the behaviour of cartilage is the proteoglycan,

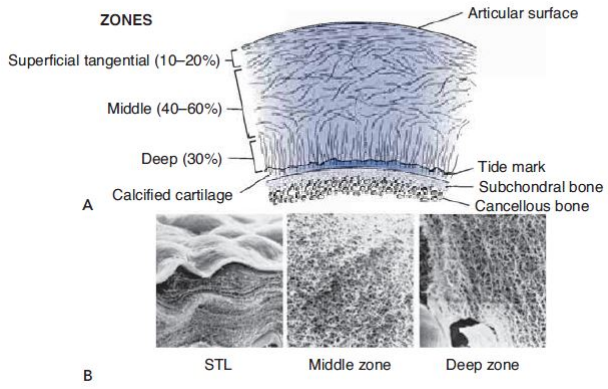

Figure 2.3: A. Schematic representation of the collagen fibers in the articular cartilage. B. Micrographs of the superficial tangential zone (STZ), of the middle zone and of the deep zone [3].

which is a large protein-polysaccharide molecule consisting of a long protein core (usually hyaluronic acid) to which many long unbranched polysaccharides, called glycosaminoglycans (GAG), are attached. The most abundant GAGs are chondroitin sulfate (CS), dermatan sulfate (DS) and keratan sulfate (KS). The actual structure is slightly more complicated: usually a CS chain and a KS chain are covalently bonded and around 150 of this polysaccharidic groups are linked to a protein backbone. This complex is called aggrecan and several aggrecans (up to some hundreds) are finally attached to a bigger protein chain such as HA. There is a strong linkage between HA and aggrecans by means of a binding protein. This is crucial to prevent components of the PG molecules from escaping the tissue.

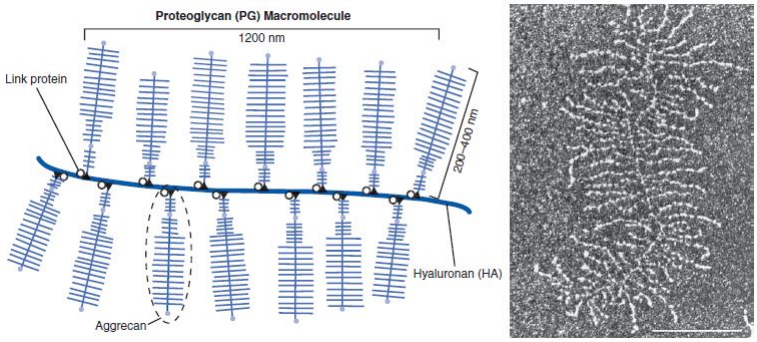

Figure 2.4: The structure of a proteoglycan. The aggrecans, consisting of GAGs attached to a protein chain, are connected to a bigger protein backbone giving the macromolecule. The structure is also visible in the transmission electron microscopy image [3].

The proteoglycans play an important role thanks to the presence of an overall negative charge distribution given by the sulfate and carboxyl groups, SO_4^{2-} and COO^- respectively. There are mainly three consequences arising from this net negative charge: PGs electrostatically attract water molecules, attract also positive

counter ions such as sodium or calcium ions and finally experience repulsive forces with each other. Both the direct affinity with water molecules and the osmotic pressure resulting from the excess of positive ions help in giving the cartilage the properties of a swollen material. The repulsive forces help in reacting to compressive loads. The more water escapes the structure under compression the more PGs get near to one another and the more this electrostatic repulsion hinder further crushing. Proteoglycans are also thought to have a role in keeping the ordered structure of the collagen fibers.

2.1.3 Biomechanical behaviour

Collagen fibers and proteoglycans interact to give a porous and permeable matrix that is swollen by water and thus capable of bearing high compressive stresses.
The commonly accepted model of the articular cartilage is of a biphasic material having two intrinsically incompressible [4] and immiscible phases, that are the porous matrix and the permeant fluid. This, as will be discussed later, is the reason why poroelasticity has been widely used to model the mechanical behaviour of this tissue.
First of all, though, articular cartilage has also typical viscoelastic features: creep, stress relaxation, hysteresis in the loading-unloading curve. All the natural tissues present a viscoelastic response but as for tendons, ligaments and bone this is single-phase viscoelasticity consequent to the sliding of the collagen fibers (tendons and ligaments) or of the osteons (bone). For articular cartilage the origins of the viscoelasticity have to be sought in the flow of interstitial fluid. The role of the fluid pressurization is extremely important especially in the impulsive response of the joints, subjected to high stresses (of the order of 20 MPa) during gestures such as jumping or running.
Under compressive creep conditions articular cartilage respond in two subsequent steps. At first there is the interstitial fluid exudation and a consequent large creep deformation. Then the deformation reaches a saturation level when the compressive stress inside the tissue reaches the same level as the applied load. The relaxation time, though dependent on the stress, is quite large and it can reach several hours [3]. It is also shown that it ranges as the square of the cartilage thickness.
The biomechanical behaviour of articular cartilage has been described with increasing complexity over the years. At first in terms of a linear elastic solid (Hirsh, 1944), then using viscoelasticity (Hayes and Mockros, 1971), then with poroelasticity and finally using the poroviscoelastic theory. A short overview of these four theories will be given at a later stage. As already mentioned, the deformational response of the articular cartilage comes both from the movement, friction, exuda-

tion and pressurization of the interstitial fluid (and this is the most important part) and from the viscoelastic features of the organic matrix. A linear elastic model is clearly inappropriate, the viscoelastic approach tries to combine both the aspects into a system of elastic and viscous elements but fails in recognizing their relative importance whereas finally poroelasticity cannot include the matrix contribution. The most appropriate theory is poroviscoelasticity, even though it is also the most complicated one.

It is worth noting that from an experimental point of view this two responses, of the interstitial fluid and of the collagen matrix, can somewhat be separated. Tensile and compressive loadings imply a volumetric change in the specimen thereby causing the fluid to flow while the matrix response superimposes to it. Therefore articular cartilage presents biphasic tensile and compressive viscoelasticity. However under pure shear loading the resulting deformation is purely given by a change in shape and not in volume. This means that only the solid collagen-PG matrix, in this case, reacts to the applied load and there is decoupling between the absent fluid response and the present matrix response. Dynamic loading experiments have been carried out to measure two viscoelastic parameters of the solid matrix of normal bovine articular cartilage (Hayes and Bodine, 1978, Zhu et al., 1993): the magnitude of the dynamic shear modulus, defined as the square root of the sum of the squared elastic storage modulus and of the squared viscous loss modulus; and the phase shift angle, whose tangent is the ratio between loss and storage modulus (see the introduction to viscoelasticity).

$$|G^*|^2 = (G^{'})^2 + (G^{''})^2 \tag{2.1}$$

$$\delta = tan^{-1}\frac{G^{''}}{G^{'}} \tag{2.2}$$

They found values ranging from 1 to 3 GPa for the dynamic shear modulus and angles from 9° to 20° for the phase shift angle.

As already mentioned the cartilage has viscoelastic features and this is the reason why it has been thoroughly studied as a viscoelastic material.

This approach can be alternative to the one that tries to find a function to interpolate the data starting from them, instead of starting from a model. Many attempts have been done in this sense. Just as an example from the modelling of soft tissues, the constitutive equations presented in table 1 can be found in the literature.

Of course this empirical approach can follow correctly the experimental data but lacks in understanding the physical mechanisms underlying their trend. One could instead try to assign each parameter, for example in the viscoelastic models, to a specific mechanism or microstructural response (fibers gliding or stretching, fluid

$\epsilon^2 = aT^2 + bT$	Tendons
$\epsilon = aT^b$	Collagen fibers
$T = a(\epsilon - \epsilon^2)e^{b\epsilon}$	Anterior cruciate ligament
$T = a(e^{b\epsilon} - 1)$	Articular cartilage

Table 1: Various experimental relations for soft tissues [5]. T is the tensile stress, ϵ is the resulting strain, a ans b are empirical constants.

flow, etc).
In any case it should be noted that the full description of the biomechanical behaviour of articular cartilage is beyond the purpose of this work. It is however instructive to point out that there are many similarities between the response of the cartilage and that of water-infiltrated polymeric fabrics, used as scaffolds, and this is the reason why these materials have a great importance in the treatment of cartilage related diseases.
Moreover this introduction justifies also why in the study of the scaffolds some aspects that may be considered secondary at first sight should be addressed. For example the fluid viscosity, which is affected by the presence of the internal distribution of charges, or the resulting fluid motion. It is not only important because it affects the mechanical response of the body but also because it is essential if in future developments cells are planned to be added, given the fact that cartilage itself is not vascularized.

2.2 Biomaterials

A biomaterial is defined by the American National Institure for Health (NIH) as any substance, or combination of substances, other than drugs, synthetic or natural in origin, which can be used for any period of time, which augments or replaces partially or totally any tissue, organ or function of the body, in order to maintain or improve the quality of life of the individual.
This is quite a general definition that implies the concept of biocompatibility, which underwent a series of modifications while trying to follow the progresses in the field. It started during the years between 1940 and 1980 considering a biomaterial as suitable as its capability of non interacting with the host but the importance of an active interaction between the human body and the biomaterial led to the following and currently accepted definition by Williams (1987): *Biocompatibility refers to the ability of a material to perform with an appropriate host response in a specific situation*[6].
When we refer to biomaterials in orthopedics, besides the biocompatibility also

further requirements are needed. Considering for example a joint replacement device a combination of strength, toughness, corrosion resistance, hardness and stiffness must be achieved.

2.2.1 Polymeric scaffolds

In the rapidly developing world of biomaterials engineering there is a great interest on fibrous polymeric scaffolds. The term *scaffold* is taken from the constructions world and it means *supporting* structure. By extension in the field of implantable devices it means the artificial structure that is needed as a support with a view, usually, of a future cell proliferation. The most common usage of scaffolds is in regenerative medicine, or *tissue engineering*. The main idea is to have a support onto which the cells are rapidly attaching and growing, thereby reproducing the portion of original tissue in case it had been damaged. There are several ways to try to achieve this. First of all the cells can be already seeded *in vitro*, some time is left them to proliferate and to start producing the extra cellular matrix and only then the scaffold is implanted; or else the artificial device can be directly placed *in vivo* if its activity is high enough in order to have cell infiltration directly from the patient's surrounding cells. Secondly, the original structure can be either biodegradable or stable in time. Of course the first option has to be pursued if the final objective is to fully regenerate the original tissue but this adds the problem of finding the correct material with the needed biocompatibility and also with the right degradation time. On the other hand the second option requires attention to the longterm behaviour of the material when in contact with the human environment with all its complexity and chemical variability. Another important aspect is that care must be taken in stimulating also the angiogenesis within the new tissue otherwise both eventual seeded cells and infiltrating new ones will die shortly by hypoxia. An important exception to this requirement is represented by articular cartilage applications. In fact this particular tissue, at least in the superficial zones where the damages are usually more severe, is not vascularized. In this case the oxygen and nutriment supply for the chondrocytes, though little is needed, is only guaranteed by the flow of the interstitial fluid in and out of the structure. For this reason the fluid dynamics in this scaffolds is relevant and it will partly be addressed in this work.
One of the most studied and promising polymers in tissue engineering is poly lactic acid, formally the polyester of lactic acid $CH_3COHCOOH$. It is a biodegradable polymer though its degradation time is dependent on many factors, for example the crystallinity degree that can be variable since the polymerization can involve both the left (L) and righr (R) optical isomers of lactic acid. Only with high fractions of

the R or L isomer this polymer is highly crystalline. The usual PDLLA is amorphous. It is also hydrofilic.

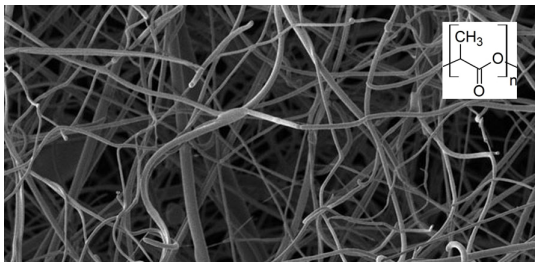

Figure 2.5: Scanning electron microscope image of a PLA polymeric scaffold showing also the molecular structure of the chain.

The object of study of this work is the behaviour of fibrous scaffold when immersed in water. This class of materials is challenging to be characterized. Macroscopically they present viscoelastic features and so this is the simplest description that can be used. Increasing in complexity there is the theory of poroelasticity or, as an alternative, empirical relations have been found.

3 Mechanical models

3.1 Linear elasticity

The theory of linear elasticity is a branch of the continuum mechanics which studies the relation between stress and strain in a body where this relation is linear. This is usually as realistic as the displacement from the equilibrium is small. At zero stress the deformation must be zero and all the quantities are not dependent on time.
Stress is a physical quantity defined point by point as the internal forces exchanged between neighbouring volume elements of the material. Mathematically it is represented by the 3x3 Cauchy tensor containing information on both normal and shear stresses. In particular the normalized force required to keep a section of the body in static equilibrium is the obtained by the application of the Cauchy tensor to the versor normal to the section itself.

$$\mathbf{t} = \sigma \cdot \mathbf{n} \tag{3.1}$$

Three fundamental equations for the solution of the problem are obtained issuing the total balance of the forces acting on an infinitesimal volume element subjected to the presence of the neighbouring elements and to eventually a body force $\mathbf{f} = [f_1, f_2, f_3]$. As often done in theories regarding elasticity $\mathbf{r} = (x, y, z)$ is replaced by $\mathbf{x} = (x_1, x_2, x_3)$.

$$\sum_{i=1}^{3} \frac{\partial \sigma_{ij}}{\partial x_i} + f_j = 0 \qquad j = 1, 2, 3 \tag{3.2}$$

With $\sigma_{ij} = \sigma_{ji}$.
Strain is defined in terms of the spatial derivatives of the three components of the displacement vector $\mathbf{u} = [u_1, u_2, u_3]$ as

$$\epsilon_{ij} = \frac{1}{2}\Big(\frac{\partial u_i}{\partial x_j} + \frac{\partial u_j}{\partial x_i}\Big) \qquad i, j = 1, 2, 3 \tag{3.3}$$

With $\epsilon_{ij} = \epsilon_{ji}$.
The other equations that are needed to solve the problem come from the constitutive equation, which is the correlation between stress and strain by the intrinsic properties of the material. This is done by introducing the elastic tensor $\mathbf{E}$, which in general is a 3x3x3x3 tensor with 81 constants. Due to the fact that this tensor is symmetric ($E_{ijkl} = E_{jilk}$) the independent components reduce to 54. Then, due to the invariance of the strain energy density function $E_{ijkl}\epsilon_{ij}\epsilon_{kl}$ when swapping ij and

kl ($E_{ijkl} = E_{klij}$) it is reduced to 21, which is the number of independent constants in a 6x6 symmetric matrix. Finally, with the assumption that the body is isotropic it eventually reduces to 2 constants only (E, ν). The constitutive equation in the case of a isotropic linear elastic body then reads (see e.g. the book by Capurso [7] for a thorough derivation)

$$\epsilon_{ij} = \frac{1+\nu}{E}\,\sigma_{ij} - \frac{\nu}{E}\,\delta_{ij}\sigma_{kk} \tag{3.4}$$

This equation can be inverted taking the inverse of the elastic tensor, i.e. a measure of the compliance of the body giving

$$\sigma_{ij} = \frac{E}{3(1-2\nu)}\,\delta_{ij}\,\epsilon_{kk} + \frac{E}{1+\nu}\left(\epsilon_{ij} - \frac{1}{3}\,\delta_{ij}\epsilon_{kk}\right) \tag{3.5}$$

3.2 Linear viscoelasticity

With the theory linear viscoelasticity the behaviour of materials whose properties involve also the time variable can be modelled. As can be seen looking at the name the combination of an elastic and of a viscous response is involved.
The main goal of this theory is to find a constitutive equation, which is a relation between stress and strain. Unlike linear elasticity in this case the time dependence makes so that also the time derivatives of stress and strain could appear in the description of the material.
The importance of this theory lies with its ability of explaining some peculiar phenomena that characterize viscoelastic materials. The most important are:

- Creep, deformation at fixed stress.
- Stress relaxation, at fixed strain.
- Hysteresis in the stress-strain curve.

During a creep experiment the applied stress σ_0 is held constant while the evolution of the strain $\epsilon(t)$ is followed. From this two quantities the following functions are of interest. The *creep compliance* is defined in one dimension as

$$D(t) = \frac{\epsilon(t)}{\sigma_0} \tag{3.6}$$

And its inverse, the *creep modulus*

$$E(t) = \frac{\sigma_0}{\epsilon(t)} \tag{3.7}$$

During a relaxation experiment an initial strain ϵ_0 is applied and the relaxation of the stress $\sigma(t)$ is followed. From this two quantities the following functions are of interest. The *relaxation modulus* is defined as

$$E(t) = \frac{\sigma(t)}{\epsilon_0} \tag{3.8}$$

And its inverse, the *relaxation compliance*

$$D(t) = \frac{\epsilon_0}{\sigma(t)} \tag{3.9}$$

The third simple loading condition that is usually used to characterize a viscoelastic material is the sinusoidal loading, or dynamic mechanical analysis. This means to observe the response of the specimen when subjected to a periodic loading at a given frequency ω. The resulting deformation, though shifted of a phase angle, maintains the same frequency. Consequently the *dynamic modulus* can be defined as

$$E^*(\omega) = \frac{\sigma(\omega)}{\epsilon(\omega)} \tag{3.10}$$

The dynamic modulus is typically derived by making the following assumptions: a sinusoidal forcing function $\epsilon(t) = \epsilon_a e^{i\omega t}$ is applied, and it will cause the stress in the material to be also sinusoidal, in particular the strong hypothesis is that the frequency of the response is the same as the forced strain, only shifted of a phase angle δ, i.e. $\sigma(t) = \sigma_a e^{i(\omega t+\delta)}$. This will allow the simplification from the time and frequency variables to the sole frequency dependence.
The objective of the dynamic mechanical analysis is to find the transfer function $E^*(\omega)$ between stress and strain as a function of the frequency and of the material constants. Starting from its definition and using the hypothesis above the complex modulus simplifies to the stress to strain amplitude ratio times a phase shift factor

$$E^*(\omega) = \frac{\sigma_a e^{i(\omega t+\delta)}}{\epsilon_a e^{i\omega t}} = \frac{\sigma_a}{\epsilon_a} e^{i\delta} \tag{3.11}$$

This is a complex function and as such separable into two contributions, real and imaginary

$$E^* = E^{'} + iE^{''} \tag{3.12}$$

Here $E^{'}$ is defined as *storage modulus*, $E^{''}$ is defined as *loss modulus* and i is the imaginary unit. Combining the two definitions and making use of the Euler equivalence δ is found to be dependent on the loss modulus to storage modulus ratio:

$\frac{\sigma_a}{\epsilon_a}\cos(\delta) + i\frac{\sigma_a}{\epsilon_a}\sin(\delta) = E^{'} + iE^{''}$ from which

$$\tan(\delta) = \frac{E^{''}}{E^{'}} \tag{3.13}$$

The names of these two parts of the complex modulus come from the fact that it can be demonstrated by integration of the element of specific energy $\sigma\partial\epsilon$ over one quarter and one period that the total elastically stored energy is $E^{'}\epsilon_a^2/2$, proportional to the storage modulus, while the total dissipated energy by viscous processes is $\pi E^{''}\epsilon_a^2$, proportional to the loss modulus.
In all these cases, the term *linear* implies that the various moduli and compliances are independent of the amplitude of the input, e.g. σ_0 or ϵ_0, and properties uniquely of the material. Like in many other cases, the linearity is often present in the range of the small deformations and seldom found in the range of the large deformations.
In order to derive the constitutive equations, the first step is to define a so called viscoelastic model. There are many of them, but they are mainly various combinations of two simple elements: a linear spring that accounts for the elastic part of the response and a linear dashpot that accounts for the viscous part of the response.
A linear spring is subjected to the Hook's law that links the applied stress to the resulting strain by means of an elastic constant that has the dimensions of a pressure (Pa).

$$\sigma = k\,\epsilon \tag{3.14}$$

A linear dashpot is described by Newton's law of viscosity, which links the applied stress to the first temporal derivative of the strain by means of a constant (in Pa·s).

$$\sigma = c\,\dot{\epsilon} \tag{3.15}$$

3.2.1 Viscoelastic models

There is a great variety of viscoelastic models that can be used to model the time dependent response of materials. They are all generalized electric circuits where the springs have the same equation as capacitors and the dashpots have the same equation as resistances. The inertial effects, modelled with inductors, are neglected. The models consist of series and parallels and there is in principle no limit in the number of elements. Of course adding elements means adding degrees of freedom for data fitting but makes also the constitutive equations more and more complicated and eventually not analytically solvable. This is the reason why the most used models are also the simplest, given that they are capable of giving the viscoelastic features of interest. The point of using viscoelastic models instead of simply searching for

some polynomial or in general any fitting curve is that physical unterpretations can be given for the elastic or viscous elements. Just to make an example from the application of the Burgers model (cfr. 3.2.3) to polymer science, the isolated elastic element is representative of the instantaneous change in bond angle and length while the isolated viscous element accounts for the long-time chains flow while finally the combined presence of the spring and dashpot in parallel represents the uncoiling of the chains.

3.2.2 Zener model

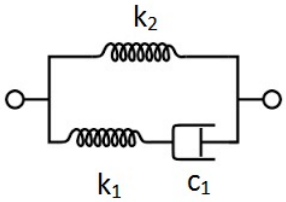

Figure 3.1: Zener model

This is the simplest model capable of showing creep, instantaneous elastic deformation and stress relaxation. It is composed of a spring in parallel to a second spring and a dashpot in series, as it can be seen in fig. 3.1. Let k_1 and c_1 be the elastic and viscous part of the series, and k_2 be the elastic component on the other side of the parallel. Due to the formal equivalence between the equations relating stress and strain and the equations relating force and displacement, in this section as well as in the next one the derivation regards the latter relation but the conclusion, needed for the actual data analysis, is about the former one. For the sake of readability new symbols are not defined even if the normalization changes the units of measure.
The equations relative to each element are

$$\begin{aligned} F_{k_1} &= k_1 x_{k_1} \\ F_{c_1} &= c_1 \dot{x}_{c_1} \\ F_{k_2} &= k_2 x_{k_2} \end{aligned} \tag{3.16}$$

Since k_1 and c_1 are in series $F_{k_1} = F_{c_1} = F_1$ and $x_{k_1} + x_{c_1} = x_1$ while from the parallel one has $F = F_{k_1} + F_{k_2} = F_{c_1} + F_{k_2}$ and $x = x_1 = x_2$.
Differentiating the last equation with respect to the time is the first step to derive the constitutive equation of the model, i.e. the relation between stress and strain (or force and displacement)

$$\dot{x}_{k_1} + \dot{x}_{c_1} = \dot{x}_{k_2} \tag{3.17}$$

Which, using the equations relative to each element, is

$$\frac{\dot{F}_{k_1}}{k_1} + \frac{F_{c_1}}{c_1} = \dot{x}_{k_2} \tag{3.18}$$

$$\frac{\dot{F} - k_2\dot{x}}{k_1} + \frac{F - k_2 x}{c_1} = \dot{x} \tag{3.19}$$

Rearranging the terms the previous equations read

$$c_1\dot{F} + k_1 F = c_1(k_1 + k_2)\dot{x} + k_1 k_2 x \tag{3.20}$$

Under a constant creep force F_0 the term $c_1\dot{F}$ disappears and the evolution of the deformation is described by the following differential equation, where the time constant is defined as $\tau = c_1(k_1 + k_2)/k_1 k_2$.

$$x + \tau\dot{x} = \frac{F_0}{k_2} \tag{3.21}$$

This is an inhomogeneous first-order ordinary differential equation. The solution $x(t)$ will be the sum of the solution of the homogeneous equation

$$x + \tau\dot{x} = 0 \tag{3.22}$$

Which is

$$x(t) = Ae^{-\frac{t}{\tau}} \tag{3.23}$$

Plus the particular integral, which leads to the complete solution that is

$$x(t) = Ae^{-\frac{t}{\tau}} + \frac{F_0}{k_2} \tag{3.24}$$

The initial condition is that at $t = 0$ both the springs react immediately while the dashpot is infinitely rigid so $x(0) = F_0/(k_1 + k_2)$ and the constant A can be determined.

$$A + \frac{F_0}{k_2} = \frac{F_0}{k_1 + k_2} \tag{3.25}$$

$$A = -\frac{k_1}{k_2(k_1 + k_2)}F_0 \tag{3.26}$$

The creep response of the Zener model is

$$x(t) = (\frac{1}{k_2} - \frac{k_1}{k_2(k_1 + k_2)}e^{-\frac{t}{\tau}})F_0 \tag{3.27}$$

The creep modulus $E(t)$ is given by

$$E(t) = \left(\frac{1}{k_2} - \frac{k_1}{k_2(k_1 + k_2)} e^{-\frac{t}{\tau}} \right)^{-1} \tag{3.28}$$

The three parameters can be obtained by a nonlinear fitting of experimental data. The dynamic response for the model is obtained plugging the harmonic stress and strain into equation 3.20 that becomes

$$(c_1 i\omega + k_1)\sigma_a e^{i(\omega t+\delta)} = (c_1(k_1 + k_2)i\omega + k_1 k_2)\epsilon_a e^{i\omega t} \tag{3.29}$$

The expression for the complex modulus is directly available, using the basic relation $(a + ib)(a - ib) = (a^2 + b^2)$, as

$$E^*(\omega) = \frac{c_1(k_1 + k_2)i\omega + k_1 k_2}{c_1 i\omega + k_1} = \frac{k_1^2 k_2 + c_1^2(k_1 + k_2)\omega^2 + ic_1 k_1^2 \omega}{k_1^2 + c_1^2\omega^2} \tag{3.30}$$

Here one can identify the storage modulus and the loss modulus

$$E^{'}(\omega) = \frac{k_1^2 k_2 + c_1^2(k_1 + k_2)\omega^2}{k_1^2 + c_1^2\omega^2} \tag{3.31}$$

$$E^*(\omega) = \frac{c_1 k_1^2 \omega}{k_1^2 + c_1^2\omega^2} \tag{3.32}$$

It is instructive to check the limits for very low and high frequencies because it must be that under quasi static force the dashpot nullify the reaction of the whole Maxwell branch whereas under high frequency loads the same dashpot is indefinitely rigid making the model to behave like just two springs in parallel.

$$\lim_{\omega \to 0} E^*(\omega) = \frac{k_1^2 k_2}{k_1^2} = k_2 \tag{3.33}$$

$$\lim_{\omega \to \infty} E^*(\omega) = \frac{c_1^2(k_1 + k_2)}{c_1^2} = k_1 + k_2 \tag{3.34}$$

As expected.

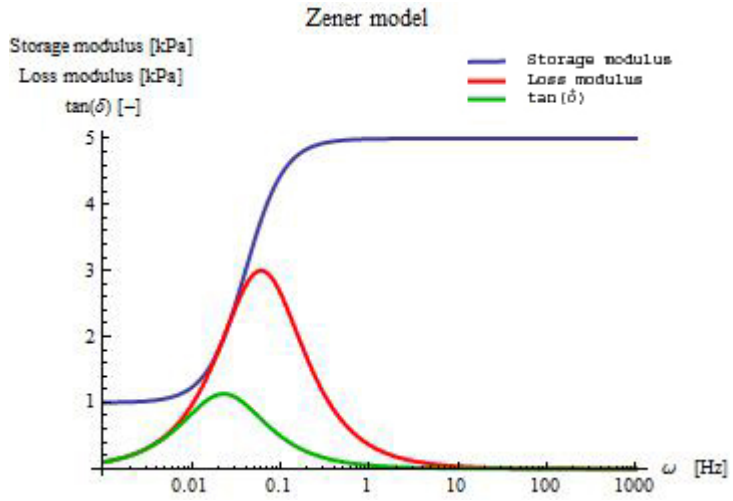

Figure 3.2: Frequency response of the Zener model with assuming $k_1 = 4$ kPa, $c_1 = 50$ kPa·s, $k_1 = 1$ kPa.

3.2.3 Burgers model

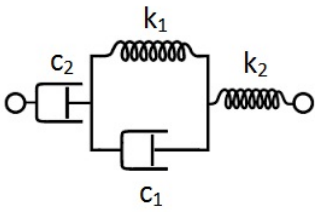

Figure 3.3: Burgers model

Consider the Burger or four-element model in fig 3.3. It is constituted by a Kelvin and a Maxwell model in series. Let k_1 and c_1 be the elastic and viscous part of the parallel, and k_2 and c_2 be the elastic and viscous part of the series.
The equations relative to each element are

$$\begin{aligned} F_{k_1} &= k_1 x_{k_1} \\ F_{c_1} &= c_1 \dot{x}_{c_1} \\ F_{k_2} &= k_2 x_{k_2} \\ F_{c_2} &= c_2 \dot{x}_{c_2} \end{aligned} \tag{3.35}$$

Where according to the common rules for the series and the parallels
$x_{k_1} = x_{c_1} = x_1$ and $F_{k_2} = F_{c_2} = F_{k_1} + F_{c_1} = F$.
The derivation of the constitute equation can start by the definition of total displacement, then differentiated with respect to the time

$$x = x_1 + x_{k_2} + x_{c_2} \tag{3.36}$$

$$\dot{x} = \dot{x}_1 + \dot{x}_{k_2} + \dot{x}_{c_2} \tag{3.37}$$

Now by substitution from equations 3.35

$$\dot{x} = \frac{\dot{F} - c_1\ddot{x_1}}{k_1} + \frac{\dot{F}}{k_2} + \frac{F}{c_2} \tag{3.38}$$

And differentiating again the first line in equations 3.35, inverting to isolate $\ddot{x}_1$ and substituting again for the forces where needed the final constitutive equation reads

$$\dot{x} = \frac{\dot{F} - c_1(\ddot{x} - \frac{\ddot{F}}{k_2} - \frac{\dot{F}}{c_2})}{k_1} + \frac{\dot{F}}{k_2} + \frac{F}{c_2} \tag{3.39}$$

After rearranging the terms it becomes

$$F + \Big(\frac{c_1}{k_1} + \frac{c_2}{k_1} + \frac{c_2}{k_2}\Big)\dot{F} + \frac{c_1 c_2}{k_1 k_2}\ddot{F} = c_2\dot{x} + \frac{c_1 c_2}{k_1}\ddot{x} \tag{3.40}$$

The constitutive equation can be higly simplified if a known constant force is given as an input. Let F_0 be the constant force applied in a creep experiment. This leads to the differential equation from which the creep function can be derived

$$\dot{x} + \frac{c_1}{k_1}\ddot{x} = \frac{F_0}{c_2} \tag{3.41}$$

Which is an explicit second-order ordinary differential equation. Since it is an inhomogeneous equation the solution $x(t)$ will be composed by the complementary function of the corresponding homogeneous equation

$$\dot{x} + \frac{c_1}{k_1}\ddot{x} = 0 \tag{3.42}$$

Which is

$$x(t) = \Big[\frac{F_0}{k_1}(1 - e^{-\frac{t}{\tau}}) + \frac{F_0}{k_2}\Big] \tag{3.43}$$

Plus the particular integral, which leads to the complete solution that is

$$x(t) = \Big[\frac{F_0}{k_1}(1 - e^{-\frac{t}{\tau}}) + \frac{F_0}{k_2} + \frac{F_0}{c_2}t\Big] \tag{3.44}$$

Where $\tau = c_1/k_1$ is the relaxation time.
From this solution an expression for the creep modulus $E(t)$ is derived as

$$E(t) = \left(\frac{1}{k_1}(1 - e^{-\frac{t}{\tau}}) + \frac{1}{k_2} + \frac{t}{c_2}\right)^{-1} \tag{3.45}$$

The 4 parameters of this model can be determined performing a nonlinear fitting on the experimental evolution of the deformation of the specimen over the time.
As far as the dynamic response is concerned, the same considerations made for the Zener model still apply. Just for convenience a more compact notation is used, re-writing the constitutive equation in terms of four constants that are the four constants multiplying the time derivatives of stress and strain in eq 3.40: $\sigma + a_1\dot{\sigma} + a_2\ddot{\sigma} = b_1\dot{\epsilon} + b_2\ddot{\epsilon}$. Assuming both sinusoidal and isofrequency forcing input and resulting output the constitutive equation gives

$$(1 + i\omega a_1 - \omega^2 a_2)\sigma_a e^{i(\omega t+\delta)} = (i\omega b_1 - \omega^2 b_2)\epsilon_a e^{i\omega t} \tag{3.46}$$

After some algebraic passages one has

$$E^*(\omega) = \frac{b_2\omega^2 - i\omega b_1}{a_2\omega^2 - 1 - i\omega a_1} \tag{3.47}$$

That brings to the following relations for the storage and loss moduli, respectively

$$E^{'}(\omega) = \frac{(a_1 b_1 - b_2)\omega^2 + a_2 b_2 \omega^4}{1 + (a_1^2 - 2a_2)\omega^2 + a_2^2\omega^4} \tag{3.48}$$

$$E^{''}(\omega) = \frac{b_1\omega + (a_1 b_2 - a_2 b_1)\omega^3}{1 + (a_1^2 - 2a_2)\omega^2 + a_2^2\omega^4} \tag{3.49}$$

The expected behaviour at very low frequency is that the Maxwell dashpot allows an everlasting deformation, putting the overall rigidity of the system to zero, while at very high frequencies both the dashpots have infinite stiffness, the consequence being that also the Kelvin spring is frozen out. Only the Maxwell elastic part should remain. Indeed

$$\lim_{\omega\to 0} E^*(\omega) = 0 \tag{3.50}$$

$$\lim_{\omega\to\infty} E^*(\omega) = \frac{b_2}{a_1} = \frac{c_1 c_2}{k_1}\frac{k_1 k_2}{c_1 c_2} = k_2 \tag{3.51}$$

3.3 Poroelasticity

Poroelasticity, or elasticity of fluid-infiltrated porous solids, is part of poromechanics, which in turn is a branch of continuum mechanics studying the behaviour of a biphasic system composed by a solid matrix having an interconnected network of pores filled by a fluid. The theory of poroelasticity assumes that the matrix is purely elastic and that the fluid is purely viscous. This theory has been mainly developed

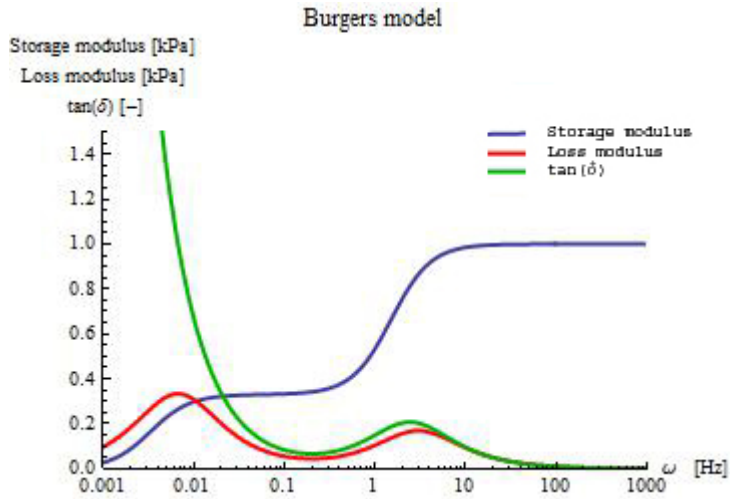

Figure 3.4: Frequency response of the Burgers model assuming $k_1 = 0.5$ kPa, $c_1 = 1$ kPa·s, $k_2 = 1$ kPa, $c_2 = 100$ kPa·s. Unlike the Zener model, the Burgers model has two different critical frequencies, associated with two inflexion points in E' and two peaks in E''.

to study rocks and soils but it has broadly used in the field of biological tissues and biomaterials.

The first general description of poroelastic materials is known as Biot's theory [8], developed by Anthony Biot between 1935 and 1957. The general idea is that there are two mechanisms accounting for the deformational behaviour: an increase in pore pressure causes the dilatation of the matrix and a compression of the matrix causes an increase of the pore pressure, if the fluid cannot escape from the pores (so called *undrained* conditions), or a fluid mass transport if the fluid can exit the structure (*drained* conditions). The coupling of this mechanisms result in an apparent time-dependent character of the matrix's mechanical properties [9] that is used, for instance, for the description of the progressive settlement of soil under its own weight and/or under the weight of shallow layers.

Biot's theory, as it will be shown, combines the classical linear elasticity equations for the solid matrix and Darcy's law, an equation for the flow of a viscous fluid inside a porous matrix that is derived starting from the Navier-Stokes equations. The variables of the problem are the three components of the displacement vector field of the body $\mathbf{u} = [u_1, u_2, u_3]$ and the scalar field of pressure $p(\mathbf{x})$. This brings to a 4x4 system of partial differential equations.

3.3.1 Constitutive equations

The main idea is first to derive a stress-strain-pressure relation valid for porous elastic solids and then to write the same equilibrium equations used to obtain $\mathbf{u}(\mathbf{x})$ also in the case of linear elasticity, adding in this case also a fourth equation, which

is Darcy's law, since there is the additional pore pressure variable [10].
The *bulk modulus* K is defined as

$$\frac{\Delta V}{V} = \frac{\sigma_{11} + \sigma_{22} + \sigma_{33}}{3K} \tag{3.52}$$

Recalling that $\Delta V/V = \epsilon_{11} + \epsilon_{22} + \epsilon_{33}$ and using the linear elastic constitutive equation (eq. 3.4) one gets

$$K = \frac{2(1+\nu)G}{3(1-2\nu)} \tag{3.53}$$

And this can be used to re-express eq. 3.4 as

$$\epsilon_{ij} = \frac{1}{2G}\,\sigma_{ij} + \left(\frac{1}{9K} - \frac{1}{6G}\right)\delta_{ij}(\sigma_{11} + \sigma_{22} + \sigma_{33}) \tag{3.54}$$

Or its inverse as

$$\sigma_{ij} = 2G\epsilon_{ij} + \left(K - \frac{2G}{3}\right)\delta_{ij}(\epsilon_{11} + \epsilon_{22} + \epsilon_{33}) \tag{3.55}$$

If also a pore pressure p is present the previous equation can be generalized considering that an increase in the pore pressure will increase only the normal stresses (Kronecker delta) and increase them in compression (minus sign).

$$\sigma_{ij} = 2G\epsilon_{ij} + \left(K - \frac{2G}{3}\right)\delta_{ij}(\epsilon_{11} + \epsilon_{22} + \epsilon_{33}) - \alpha\delta_{ij}p \tag{3.56}$$

α is a constant of the porous material. Solving for the strain the previous relation one has

$$\epsilon_{ij} = \frac{1}{2G}\,\sigma_{ij} + \left(\frac{1}{9K} - \frac{1}{6G}\right)\delta_{ij}(\sigma_{11} + \sigma_{22} + \sigma_{33}) + \frac{\alpha}{3K}\delta_{ij}p \tag{3.57}$$

It has to be noted that K is here considered in *drained conditions*, when the fluid exits freely the solid structure keeping its internal pressure constant. In *undrained conditions* there is the other extreme case where the fluid is prevented from flowing but pore pressure can increase. In this case the undrained compressive modulus K_u is used to give

$$\sigma_{ij} = 2G\epsilon_{ij} + \left(K_u - \frac{2G}{3}\right)\delta_{ij}(\epsilon_{11} + \epsilon_{22} + \epsilon_{33}) \tag{3.58}$$

There are two compressive moduli but only one shear modulus. This is due to the fact that shear even if in the undrained case do not induce a pressure change because it does not give volume but only shape variations.
To move further the definitions of *porosity* n and of *fluid mass content* m are needed

and they are

$$n = \frac{V_f}{V} \tag{3.59}$$

$$m = \frac{M_f}{V} \tag{3.60}$$

Where V_f and M_f are the fluid volume and mass and V is the volume at the reference unstressed state and so $m = \rho_f n$. If the material is completely soaked fluid volume and volume of pores coincide. For small variations

$$\Delta m = n\Delta\rho_f + \rho_f \Delta n \tag{3.61}$$

It can be shown that

$$\Delta m = \rho_f \alpha \left(\epsilon_{11} + \epsilon_{22} + \epsilon_{33} + \frac{\alpha}{K_u - K} p \right) \tag{3.62}$$

$$\Delta n = \alpha \left(\epsilon_{11} + \epsilon_{22} + \epsilon_{33} \right) + \left(\frac{\alpha^2}{K_u - K} - \frac{n}{K_f} \right) p \tag{3.63}$$

Where K_f is the bulk modulus of the fluid phase.
To solve the problem one more equation is required, in particular the one governing the flux of a viscous fluid inside a porous isotropic media, also known as Darcy's law. If k is the intrinsic permeability of the solid phase, and μ_f is the viscosity of the fluid, then the discharge velocity of the fluid in the solid is proportional to the gradient of the pressure

$$\mathbf{q} = -\frac{k}{\mu_f} \nabla \mathbf{p} \tag{3.64}$$

The mass of the fluid involved in this flow must be conserved and that is saying that its time derivative must be zero. Considering a monodimensional channel of cross section A and length dx with a fluid discharge velocity $q_x(x)$, the balance between entering and exiting mass is $(\partial(\rho_f q_x A)/\partial x)dx$. In addition to this there is also the possibility that fluid is uptaken or expelled because of a change in porosity, for instance given by a strain applied to the sample. This specific fluid mass variation Δm (in kg/m^3) is in general a function of time and gives a contribution to the time derivative. The conservation of mass in this simple case is $(\partial(\rho_f q_x A)/\partial x)dx + (\partial(\Delta m)/\partial t)Adx = 0$. This result can be extended to an infinetesimal volume dV giving

$$\sum_{i=1}^{3} \frac{\partial(\rho_f q_i)}{\partial x_i} + \frac{\partial(\Delta m)}{\partial t} = 0 \tag{3.65}$$

The first three partial differential equations derive from the equilibrium, the fourth is obtained combining Darcy's law and mass conservation. Starting from the equilibrium condition $\sum_{i=i}^{3}(\partial\sigma_{ij}/\partial x_i) = 0$, using eq. 3.56 to express it in terms of the strain and re-expressing it in terms of the displacements using the definition of strain one has eq. 3.66. Starting from the mass conservation law and using eq. 3.62 for Δm and eq. 3.64 for the discharge velocity q_i one has eq. 3.67

$$\left(K + \frac{G}{3}\right)\frac{\partial}{\partial x_i}\sum_{i=1}^{3}\frac{\partial u_i}{\partial x_i} + G\nabla^2 u_j - \alpha\frac{\partial p}{\partial x_j} = 0 \qquad \text{for } j = 1, 2, 3 \tag{3.66}$$

$$-\frac{k}{\mu_f}\nabla^2 p + \alpha\frac{\partial}{\partial t}\left(\sum_{i=1}^{3}\frac{\partial u_i}{\partial x_i} + \frac{\alpha}{K_u - K}p\right) = 0 \tag{3.67}$$

An interesting thing comes out doing a linear combination of the sum of the spatial derivative $\partial/\partial x_j$ of each of the first three equations (thus getting the ∇^2 operator) and of the fourth equation. The result, after algebraic manipulation is

$$c\nabla^2\left(\sum_{i=1}^{3}\frac{\partial u_i}{\partial x_i} + \frac{\alpha}{K_u - K}p\right) = \frac{\partial}{\partial t}\left(\sum_{i=1}^{3}\frac{\partial u_i}{\partial x_i} + \frac{\alpha}{K_u - K}p\right) \tag{3.68}$$

This means that the alteration of fluid mass content satisfies the equation of diffusion

$$c\nabla^2(\Delta m) = \frac{\partial}{\partial t}(\Delta m) \tag{3.69}$$

This is in fact a theory that couples deformation and diffusion.

3.3.2 Permeability

One of the important parameters that governs the behaviour of the sample in the simulations is the *intrinsic permeability* k, the constant that appears in Darcy's law. The physical meaning of this constant, whose unit of measure is m^2, is how much the fluid is free to flow inside the medium, provided the amount of viscous resistance by μ. Therefore k is a property of the porous medium only, and not of the flowing fluid. A compact definition for accounting how easily a given fluid will flow through a given structure is that of the *hydraulic conductivity* $K_{hyd} = \rho g k/\mu$, in m/s.
It is worth noting that Darcy's law was born on the basis of studies on the flow through porous beds of sand, not subjected to external stresses. In the case of scaffolds this compaction of the fibers should be taken into account since the more the structure is crushed the more the fibers get closer and therefore effective in obstructing the flow. This suggests that there must be a dependence on the applied

strain. This is sometimes formulated as the dependence of the permeability on the porosity of the system [11] rather than on the strain, but the two quantities are related to one another. In other works [14] the strain permeability correlation has been taken as exponential, using two experimental parameters, in the case of articular cartilage (eq. 3.82). Since it was not a known factor, a plausible value for the permeability needed to be extracted by the simulations. This task is easier if the relation is even simpler, and this was the motivation for the simple model presented here.

Consider a porous cylinder, infiltrated by a fluid, of height H and radius R. When compressed, the fluid will escape from the central regions toward the free vertical face. The cross section interested by the flow is therefore a cylindrical shell of area $2\pi RH$. This cross section, relative to the undeformed volume, will change when compression starts. When the height is reduced by an infinitesimal amount δH, the radius increases of δR. The relation between this infinitesimal quantities depends on the Poisson ratio. The two extreme situations are picked for simplicity. In the case of incompressible materials the volume is unchanged, and neglecting the second-order terms

$$V_0 = \pi R^2 H = \pi(R + \delta R)^2(H + \delta H) = V_f \tag{3.70}$$

Which leads to

$$\frac{\delta R}{R} = -\frac{1}{2}\frac{\delta H}{H} \tag{3.71}$$

In the case of Poisson's ratio approaching zero the relation is simply

$$\frac{\delta R}{R} = 0 \tag{3.72}$$

Now, identifying with S_0 the initial cross section $2\pi RH$ and again neglecting the second-order terms, the deformed section becomes

$$\begin{aligned} S &= 2\pi(R + \delta R)(H + \delta H) \approx 2\pi RH + 2\pi\delta RH + 2\pi R\delta H = \\ &= S_0 + 2\pi RH\left(\frac{\delta H}{H} + \frac{\delta R}{R}\right) \end{aligned} \tag{3.73}$$

For Poisson's ratio of $1/2$ and 0 this results respectively in

$$\begin{aligned} S &= S_0\left(1 + \frac{1}{2}\frac{\delta H}{H}\right) \\ S &= S_0\left(1 + \frac{\delta H}{H}\right) \end{aligned} \tag{3.74}$$

Now the hypothesis needed to go further is that the permeability is directly proportional to this cross section, i.e. $k \propto S$. This allows to correlate strain and permeability in both cases using only the parameter of the permeability in the undeformed state.

$$\begin{aligned} k = dS = k_0 \left(1 + \frac{1}{2}\frac{\delta H}{H}\right) \\ k = dS = k_0 \left(1 + \frac{\delta H}{H}\right) \end{aligned} \tag{3.75}$$

From the definition of true strain $\epsilon = \log\left(1 + \frac{\delta H}{H}\right)$ it follows that $\frac{\delta H}{H} = e^{\epsilon} - 1$ and thus, for the two considered classes of materials, the final result is

$$\begin{aligned} k = k_0 \frac{1 + e^{\epsilon}}{2} \\ k = k_0\, e^{\epsilon} \end{aligned} \tag{3.76}$$

Of course the previous equations have been derived within the hypothesis of small displacements from the initial conditions. However it is interesting to note how the incompressible materials should be less affected than those having nearly zero Poisson's ratio, and also that at high negative strains in the first case the permeability approaches 1/2 of the initial value while in the second it approaches zero (of course beyond the boundaries of physical and mathematical meaning for this reasoning).

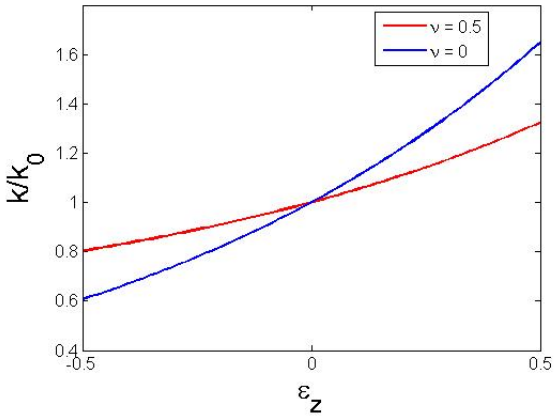

Figure 3.5: Trend for the relative intrinsic permeability as a function of the applied strain for the cases of materials having a Poisson's ratio of 1/2 or 0. Its value in both cases exponentially increases as the sample is placed in tension and exponentially decreases as the sample is compressed.

3.3.3 Parameters determination

So far the poroelastic model does not consider neither the solid nor the fluid phase as incompressible. If this hypothesis is made, then the independent constants required for the characterization of the system are four, say the drained Young's modulus, the drained Poisson's coefficient, the matrix permeability and the fluid viscosity. The following approach, valid in frictionless conditions, has been proposed by Naili *et al* to experimentally measure these parameters [16]. The quantitative results, due to different kind of experiments and different conditions, for instance regarding friction, are not here considered but the approach that will be followed is somewhat similar. Their characterization technique uses a test where at first an unconfined compression test is run, from which both the elastic constants are extracted, and secondly a stress relaxation test is performed, allowing to get a second value of the Young's modulus. The idea underlying both the tests is that even if in both cases there is a transient period, an asymptotic behaviour is reached, and with it the simplification of the relations used to describe the response. This asymptotic state is indeed under drained conditions, which means that the fluid pressure is constant over time and that the fluid can flow out of the matrix (at a rate proportional to the pressure gradient). The initial state on the other hand has typically a fluid pressure that is changing and the fluid has not reached a steady flow because it still "trapped" inside the solid. That is saying that in a simple compression test there is a change from the initial undrained to a steady drained response.
During the initial compression test, performed under controlled displacement at constant velocity v, the reaction force is calculated as the surface integral of the stress component σ_z and it has initially a complicated expression deriving from the analytical solution. The interesting fact is that this term, which is an infinite sum from zero to infinite, contains always an exponential term $\exp(-\alpha t)$ that is bound to vanish eventually. The decay time is shorter than the experimental time and therefore the asymptotical trend for the reaction is

$$F(t) = \pi a^2 E \frac{v}{h} t + (1-2\nu)^2 \pi a^4 \frac{v}{h} \frac{\mu}{k} \tag{3.77}$$

In this equation ν is extracted by the extrapolation to time equal to zero and E is calculated from the slope of the line, provided that permeability and viscosity are already known.
The asymptotic value of the reaction force is obtained again as a surface integral of the vertical stress after that it relaxed to a constant value at time approaching

infinite. This constant value is

$$F = \pi a^2 E \frac{v}{h} t_0 \tag{3.78}$$

Where t_0 is the timespan of the compression test.
In Naili's work the other two constants for Darcy's law were measured in a more conventional way. The matrix permeability k was obtained by taking measurements of the mass flow rate (by simple weighing) and at the same time of the pressure drop with a differential pressure transducer and the dynamic viscosity was measured by a capillary viscometer.
One problem that could possibly arise using this approach, as they note, is the fact that the intrinsic long term nature of these tests could bring the system too far from the hypothesis of small strains.

3.4 Poroviscoelasticity

The time dependency of the response of poroelastic systems comes from motion of the fluid inside the cavities of a purely elastic matrix. It may however be that also this matrix has an intrinsic evolution in time of its mechanical features. With the aim of separating this two contributions to the global behaviour of the material the theory of poroviscoelasticity has been developed. Poromechanics was born to study water-infiltrated rocks, and from the same field came also the motivation for this further complication of the model because after prolonged soaking some soils present viscous flows. In polymeric scaffolds, as well as in biological tissues the origin of the viscoelastic features of the matrix is completely different but also in this case these two fields found mutual advantages from the respective studies.
The modification of the poroelastic theory has to be done when the stress-strain relation was first introduced. From the linear elastic constitutive equation $\boldsymbol{\sigma} = 2G\boldsymbol{\epsilon} + \lambda \operatorname{tr}(\boldsymbol{\epsilon})\mathbf{I}$. the Lamé's constant λ can be expressed in terms of the bulk modulus K with $\lambda = K - \frac{2}{3}G$. This allows to highlight the decomposition of the stress in hydrostatic and deviatoric components, being the deviatoric tensor defined as $\operatorname{dev}(\boldsymbol{\epsilon}) = \boldsymbol{\epsilon} - \frac{1}{3}\operatorname{tr}(\boldsymbol{\epsilon})\mathbf{I}$.

$$\boldsymbol{\sigma} = K \operatorname{tr}(\boldsymbol{\epsilon})\mathbf{I} + 2G \operatorname{dev}(\boldsymbol{\epsilon}) \tag{3.79}$$

At this point instead of keeping the elastic deviatoric part $\operatorname{dev}(\boldsymbol{\epsilon})$ the time-dependent viscoelastic deviatoric strain is introduced. Only in this term since the viscoelastic influence on the volumetric part has been shown to be negligible [13]. The starting

point for the development of the new model therefore is

$$\boldsymbol{\sigma} = K\,\mathrm{tr}(\boldsymbol{\epsilon})\mathbf{I} + 2G\int_0^t F(t-\tau)\frac{\partial(\mathrm{dev}\,(\boldsymbol{\epsilon}))}{\partial\tau}d\tau \tag{3.80}$$

Where $F(t-\tau)$ is the viscoelastic relaxation function.
After this the pathway to the final partial differential equations is conceptually the same, but not in the same easy close form. However this is the starting point for the a computer simulation of poroviscoelasticity. All what is needed is to replace the constants of the model in the already implemented poroelasticity with time dependent equivalent terms.

3.4.1 Poroviscoelasticity in cartilage

When analyzing the mechanical behaviour of fluid-saturated media in soil mechanics the two elements to consider are the porous rocks and the water inside the porosity. Speaking of cartilage the situation is slightly more complicated. Instead of having a biphasic poro(visco)elasticity the it is better to consider a triphasic system since the solid phase is actually composed by a nonfibrillar matrix, the one that retains the interstitial fluid, i.e. the proteoglycans, and by a fibrillar reinforcement, i.e. the collagen fibers [14]. In this model the reinforcing fibers are considered effective only if the tissue is stressed under tension, and their contribution to the overall stiffness increases as the tensile strain increases. During compression nothing changes compared to the biphasic case. The motivation for this extension was that in such a way it was possible to explain the asymmetry in the transient response in relaxation experiments between further compression or release of the same displacement. In particular in this triphasic model two sources of nonlinearity were considered. The first lies with the elastic modulus for the collagen matrix, defined by intervals as a linear function of the strain when the strain is positive and zero when the strain is negative

$$E_f = \begin{cases} E_f^{\epsilon}\epsilon_f + E_f^0 & \epsilon_f \geq 0 \\ 0 & \epsilon_f < 0 \end{cases} \tag{3.81}$$

The second is in considering also the intrinsic permeability of the matrix as a function of the strain, being the dependence exponential

$$k = k_0\, e^{m\epsilon} \tag{3.82}$$

The loading conditions are different from those applied in the experiments which are the starting point of this thesis, and therefore the actual results are not of interest. However the method that was used is interesting and it is left as a reference, because before finding this paper the creep data had shown a linear correlation between stress and viscoelastic parameters, and a similar description the permeability had been derived.

4 Modelling methods

4.1 Finite element simulations

Computer simulations of engineering problems are becoming more and more important in almost all the scientific fields and biomedical applications do not constitute an exception. The computational approach to complex models is not new but only recently the increasing calculating capacity and the constant development of the various software have really rendered these simulations reliable. This work can only give a hint of what can be done. In the upcoming future, for example, it should be possible to integrate advanced imaging methods in order to run simulations on realistic representations of the physical objects, either actual biological tissues or scaffolds.

The need for developing finite element (FE) analysis comes from the need to solve engineering problems that, in general, are described by a system of one or more ordinary or partial differential equations. One first way is to find the analytical solution. This is usually the best way since it is possible to see the response of the system simply changing its various parameters in the closed-form solution. The problem is simply that if the geometry gets complex or there are coupled equations like in multiphysics problems, it gets soon hard to solve the problem analytically, unless heavy and not always acceptable simplifications are introduced. The second alternative approach is then to *numerically* tackle the equations starting from some initial configuration. There are several other methods (the finite difference method is the main one) but the most widely used is surely what goes under the name of *finite element method*. The main advantage of numerical methods are that by them it is possible to study complex geometries, it is possible to solve for variables that would be challenging to experimentally measure and it is easy to stimulate the system with extreme conditions, not to mention the fact that usually experiments take time and money. Of course there are also drawbacks, mostly related to the approximations that is usually necessary to make and to the fact that even if the solver reaches a solution, one must be very careful before believing it, especially when studying complex problems.

The idea behind finite element simulations is quite simple: the space is partitioned in discrete elements, depending on the nature of the problem the governing equations are written in this spatial domain and then numerically integrated starting from the conditions imposed as boundary conditions. In all the cases the mathematical problem to solve is a system of partial differential equations having one or more dependent variable(s). The solver must be given all the parameters appearing

in the equations, as well as the initial conditions for the dependent variables. If the problem is time-dependent the numerical integration is extended over the given time interval.
Of course if the rationale is simple the actual simulation, as well as the numerical analysis that calculates the solution, is not. Some of the problems can be, for instance, the generation of the geometry, the uncertainty in some of the physical constants of the equations, the correct discretization of the volume that must be detailed enough to have good results but not too refined since the computational time is greatly affected by this, especially if there are nonlinearities involved. Another important note is that if the software finds a solution it does absolutely not mean that that is the correct one. A careful validation of the model should be performed, if feasible.

Mathematically the method can be explained considering a generic variable $\phi(\mathbf{r})$, defined within a given subdomain, which represent the target unknown. It may be for instance the displacement, temperature or pressure field and in general it is a *continuous* variable. Now, just like in a continuous picture the space is made up by infinite infinitesimal volume elements here the same space is filled by a finite number of finite elements (see figure 4.1). The same equations that apply to the continuous variable $\mathbf{r}$ apply also to the *discrete* set of points defining the elements. They are called nodes and they form what is known as the mesh of the subdomain. The software tries to get the numerical solution for the nodes and then uses these values to calculate the value of ϕ for all the points of the volume, thus it is basically an interpolation. If ϕ_1, ϕ_2 and ϕ_3 are the values of the field variable in the nodes 1, 2 and 3 of a triangular element, then the field variable inside the element is

$$\phi(\mathbf{r}) = N_1(\mathbf{r})\phi_1 + N_2(\mathbf{r})\phi_2 + N_3(\mathbf{r})\phi_3 \tag{4.1}$$

Where N_1, N_2 and N_3 are called shape functions and are usually polynomial functions.
The key point is that the output of the simulation is a field function $\phi(\mathbf{r})$ just like an eventual analytical solution, but in order to get it, the space is first discretized and then re-assembled by interpolation. To have an idea of how the nodal values are calculated consider the example of a structural problem where the field function, u, is the displacement field. The starting point is the discretization of u in the discrete counterpart that is the arrow of the degrees of freedom for each node $\{U\}$. The nodal displacements are the effect of the nodal loads contained in another arrow, $\{P\}$. For each element, taking the correct elements of the global arrows, $\{U^e\}$ and $\{P^e\}$ are defined. Then the single element displacements are connected to the cor-

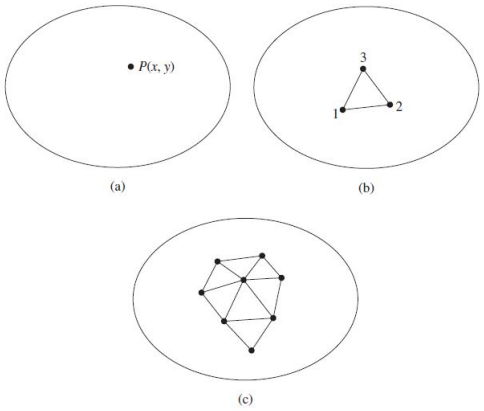

Figure 4.1: (a) General subdomain where a field variable can be defined, as well as (b) a triangular element, (c) starting point for the assembly of the mesh [12].

responding loads by the definition of a constitutive equation in the form of a matrix $[Y]$. Since the stress-strain relation is defined in the continuum mechanics first the continuum variable strain is derived by the element displacement by the usage of the matrix $[L]$ (definition of strain) that operates on the now continuum displacement field thanks to the application of the matrix of the shape functions $[N]$. Therefore the matrix $[B]$ spatial derivative of the shape functions, is defined.

$$\{\epsilon\} = [L]\,[N]\,\{U\} = [B]\,\{U\} \tag{4.2}$$

Secondly the virtual work principle is used to link cause and consequence. The internal work is

$$\mathcal{L}^i = \int_V \{\epsilon\}^T \{\sigma\}\, dV = \{U^e\}^T \int_V [B]^T [Y]\,\{\epsilon\}\, dV = \{U^e\}^T \int_V [B]^T [Y]\,[B]\, dV\, \{U^e\} \tag{4.3}$$

While the external work is

$$\mathcal{L}^e = \{U^e\}^T \{P^e\} \tag{4.4}$$

By imposing $\mathcal{L}^i = \mathcal{L}^e$ finally the desired relation is obtained by the so called stiffness element matrix.

$$\{P^e\} = \int_V [B]^T [Y]\,[B]\, dV\, \{U^e\} = [K^e]\,\{U^e\} \tag{4.5}$$

The next step is to build the stiffness structure matrix by summing the N single element matrixes (but re-written in a sparse matrix so as to satisfy the condition that nodes common to different elements need to have the same displacement, more details are contained in textbooks) as $K_{ij} = \sum_{e=1}^{N} K_{ij}^e$. This contains the condition of nodal equilibrium.

The result is a matrix that, given the nodal displacements, gives the nodal loads. Since what is usually applied, and therefore known, are the loads, the solution of the problem is in the inversion of the last matrix, i.e.

$$\{U\} = [K]^{-1} \{P\} \tag{4.6}$$

More precisely some of the nodal loads are actually known because they are the constraints necessary not to have an unstable structure. In those nodes what is unknown are the loads and thus in the last definition the left hand side contains all the nodal displacements but the constrained ones and none but the loads of the constrained nodes. The applied loads enter the right hand side of this equation.
The time consuming part of the solution is in the inversion of the matrix. For linear problems this is done only once, in the case of non linearities, which can enter for example in the definition of the constitutive equation $[Y]$ (nonlinear material) or in the defition of $[B]$ (large displacements), the inversions are several and the solution time can significantly increase.
Summarizing, the main steps are:

- Discretization of the structure
- Analysis of the single element
- Assembly of the whole structure

And after the solution the postprocessing phase begins, i.e. the extraction of all the results in the form of plots or data.

For this project *Comsol Multiphysics 3.5* has been used, a software that gives the possibility of solving coupled phenomena such as the combination of structural mechanics and fluid dynamics that governs the behaviour of fluid-saturated media. This problems in particular can be addressed using the Earth Science Module since originally the theory of poroelasticity was developed in the field of geology. In this case the dependent variables are the displacement field $\mathbf{u}(x, y, z)$ and the fluid internal pressure p. Since this is a multiphysics problem also the model has two parallel developments. For the structural mechanics model the required parameters are the mechanical properties of the matrix and the boundary conditions on both displacements and forces. This means giving the initial geometry, the constraints, eventual symmetry conditions and the external forces acting on the model. The program considers also a body load given by the interstitial fluid and evaluated from the gravitational potential as $\nabla(\rho_f g h)$. As for the fluid dynamics part the parameters are those related to the partial differential equation derived from the

Darcy's law while the boundary conditions are on the fluid flow (impervious or permeable boundaries, symmetry conditions) and on the external pressure.

4.1.1 Simulation of biological tissues

FEM simulations of soft tissues have been performed for a long time and using different material laws. An overview of material models and related problems is given in a recent review [17]. Among the time independent descriptions the simplest is the isotropic linear elastic, used in an early study on menisci. Subsequently the laws for orthotropic materials (i.e. having different properties in three orthogonal directions), and in particular the subclass for transverse isotropic ones (when two of these directions are equivalent) were considered. They proved to be effective e.g. in simulations of menisci, given its layered structure. However the linear approach is not enough if high loads are considered. For example tendons and ligaments have a typical nonlinear behaviour in tension with an initial toe region, a linear part and a final failure region. Since this is given by the first organizing and then stretching collagen fibers, fiber reinforced models were developed. Therefore they are mainly used in problems where the tissue is stressed under tension. The reinforcing phase adds the nonlinearity and one of the possibilities comes from the studies on polymeric materials and is known as the theory of hyperelasticity by Mooney and Rivlin. As already mentioned, this is particularly adequate for the analysis of tendons and ligaments.

The time dependent models, on the other hand, can consider one, two or three phases. Monophasic models use viscoelasticity, thus they consider both the causes of the time dependency, i.e. intrinsic tissue viscoelasticity and fluid exudation and imbibition, at once. For instance the Kelvin-Voigt model (a linear spring and a linear dashpot in parallel) was used for ligaments and tendons, while the Zener model (with nonlinear elements) accounted for the behaviour of the annulus fibrosus (fibrous ring of the intervertebral disk) or of the articular cartilage. The biphasic models, where the two phases are one solid and one liquid, are basically two: poroelasticity and the theory of mixture-based materials, which does not separate the two phases but associates to each volume element both the degrees of freedom for the solid and for the liquid phase. The two approaches give similar results and they can also include a fibrous reinforcement. One advantage of having an estimation of the solid phase stress is the possibility of performing failure and crack growth analysis. Finally, triphasic models include also what is called ion phase, which accounts for the osmotic swelling, caused by the ion concentration gradients that establish because of the interactions between ions and charged species. These models have a

charged solid phase (in the case of articular cartilage, negatively charged because of the proteoglycans), the fluid phase and the ion phase. Given their complexity, these models are seldom used in applied researches.

Two interesting applications of FEM analysis are the study of damage and crack propagation and the modelling of interactions. They both present practical problems. The former, especially as for articular cartilage, suffers from the long time scale that is required and from the lack of data for the validation of the model, the latter has to overcome the difficulty of the description of the contact involving at least one soft tissue. This because it is hard to have convergence in contact problems if the allowed displacements are important. Moreover if the material laws are those of poroelasticity there are no good contact algorithms since they do not consider a tangential flow that may be relevant if there is enough space between the two modelled bodies. One last problem is taking into account friction. In normal joints it is negligible but it is not in the contact for example between cartilage and hard materials (that is, in the experiments this frictionless simplification does not hold).

Many examples of applications are available in the literature. For instance early studies [18] focused on bone response when subjected to sinusoidal loading. Compact bone has multiple levels of porosity since thare is a microporosity associated with the space between the crystals of hydroxiapatite, the one associated with the canaliculi (canals between the lacunae where osteocytes live) and the mineral phase, and the bigger porosity given by the vascular structures (Haversian and Volkmann's canals). Considering only the second kind, the one deriving by the canaliculi system, they found that there is a difference both in the phase shift and in the amplitude of the harmonic fluid pressure induced by an harmonic loading of the bone. In particular to higher frequencies are associated a lower pressure amplitude and a negligible phase shift.

Other articles instead deal with cartilage For example unconfined compression and indentation can be modelled [19]. Here the material is even more precisely described as fiber-reinforced biphasic matrix. This means that the fluid saturated medium is given only by the proteoglycan matrix and the interstitial fluid, while the collagen acts as a reinforcement. They were able to see the influence of the fibers orientation in the material response including an anisotropicity that poroelasticity itself does not have. This could have interesting developments in the modelling of, for instance, menisci or intervertebral disks deformation (since both of them are organized in a peculiar fashion as for the spatial collagen fibers orientation).

As far as the modelling of the scaffolds is concerned, the challenge in the current research is to be able to generate an *exact* model of them. Instead of considering

a macroscopic body with certain material properties by using advanced 3D imaging techniques the actual fibers arrangement can be imported into the finite element softwares, meshing then this structure with 3D elements. This has already produced positive results for example in the study of tensile tests of fibrous scaffolds for ligament tissue engineering [20]. Here it was possible to generate the fibrous structure using X-ray tomography and the agreement between the experimental data and the FEM results was found to be good.

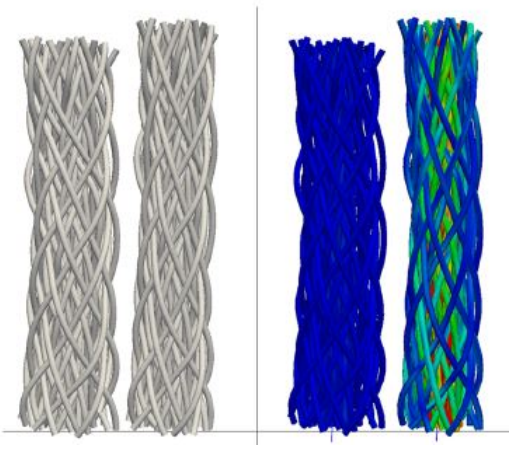

Figure 4.2: Example of the usage of 3D imaging to obtain the geometry of the simulation. In this case X-ray tomography of fibrous scaffolds for ligament tissue engineering. The imaging took place while the tensile experiment that later on would be modelled was carried on [20].

.

4.2 Experimental conditions

The computer simulations carried out in this work required also experimental data. Like in many cases, they are required both prior to and after the development of the model. As already mentioned, if the FEM analysis want to be quantitative they need to be implemented with realistic material properties. As a consequence of this the first step was the analysis of data from creep experiments performed on the scaffolds. Some experiments should also be done after the simulation gave its results, in order to validate the model.
For the tests a Netzsch DMA 242 C was used (figures 4.3 and 4.4).

(a) (b)

Figure 4.3: a) Netzsch DMA 242 C and b) representation of the sample holder for measurements in a fluid saturated environment [21].

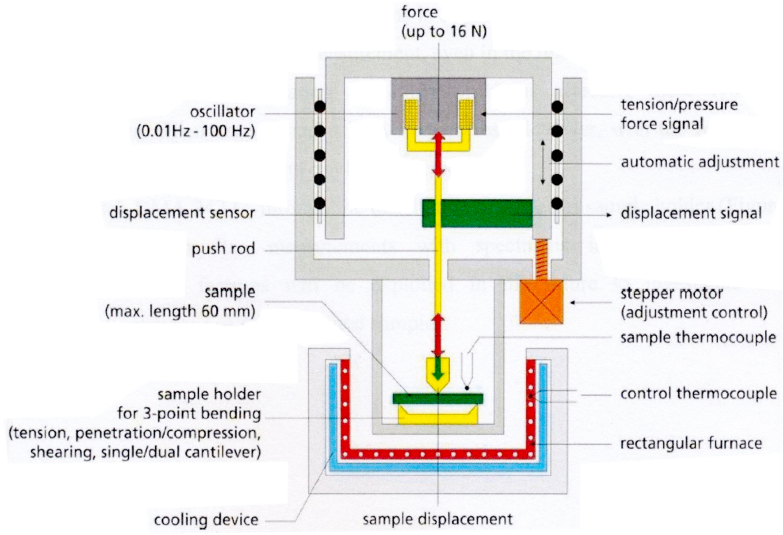

Figure 4.4: Schematic description of the machine.

This instrument can run dynamic mechanical amalysis, i.e. tests where either a sinusoidal load or a sinusoidal displacement is imposed, thereby recording the response of the material in terms of its complex modulus, in the following configurations: three-point bending, torsion, cantilever bending, tension, compression/penetration. The allowed frequency range is 0.01-100 Hz. The same apparatus can also be used for other simple loading conditions such as creep at fixed load or stress relaxation at constant displacement. The machine has a heating system to have the control over the testing temperature (from -170 ℃ to 600 ℃) and it can also be equipped with a special sample holder that allows measurements under

soaked conditions. It can be used to perform temperature scanning studies such as those involving the glass transition temperature, studies at fixed frequency, or frequency scanning analysis. The present work did not require the temperature as a variable and so the furnace was not used and the data were recorded at constant room temperature. In a further stage it may be possible to set the temperature again as a constant but at the physiological 37 ℃.
For the materials characterization samples of around 3 mm height and 10 mm diameter were used.

5 Results

5.1 Creep data fitting

In order to procede with the simulations, as well as to be able to characterize different materials, it is useful to describe their response to simple loading conditions using adequate mechanical models. Given the time dependency of the properties of fluid infiltrated solids the first and simplest way is using viscoelastic models. The chosen loading condition was creep under constant load and the data were fitted using the Zener model and the Burgers model to see which one works better and if the material can be considered as linear viscoelastic. Data on two different fabrics and creep tests at room temperature in both dry and soaked conditions were used. The first is a textile fabric while the second is the PLA scaffold. The equipment, in load control mode, was set to apply constant forces of increasing forces from 0.1 N to 3.2 N. From these experiments it emerged that a reasonable range for the characterization of this kind of materials is between 0.2 N and 0.8 N, resulting from the balance between the need of overcoming the initial arrangement of the fibers and the need not to deform the structure too much causing a sensible decrease of the porosity.
The first problem at this point is clear by the look at fig. 5.1. The (unrealistic) hypothesis underlying in the theoretical treatment of creep is that the applied force passes from zero to the constant value F_0 in a infinitesimal time, and therefore that it can be treated in the equations like a step function. In the real case it can be seen that it takes some minutes to reach the set value. This means that the material undergoes a considerable amount of deformation while the force is not what it is supposed to be yet.

This would not be a problem since the force profile can be accurately modelled as exponentially rising and the corresponding analytical solution for the strain, for instance using the Zener model, was also found. This solution, though, was not applied since the real issue is that the first part of the data on the displacement is affected by the settling of the loading system. In the DMA machine there are elements with their own stiffness that are in between the mechanical actuator and the sample, for instance the overall steel structure and the magnets. This disturbance lasts for a time comparable to the time constant of the rising of the force. The reason for this adjustment is because at the beginning of the test the pushrod needs to slightly compress the sample (of around 10 μm) to assess that the contact has been established. While the force starts to be applied this initial additional displacement is gradually removed. The manufacturer itself recommends not to use this first part of the experiment. There were no data on the stiffness of the machine, therefore a

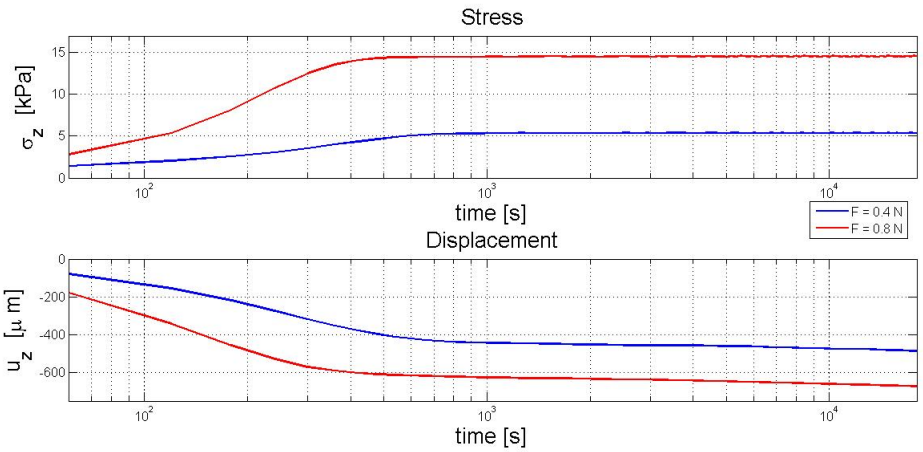

Figure 5.1: Creep experiment showing the actual stress applied at sample. The system is not able to reach immediately the desired constant value. This period of adjustment is a feature of the machine since it has been found to be independent of the set force (and consequently of the material reaction). In this figure, as an example, the measured stresses and resulting vertical displacements are plotted against time in logarithmic scale for two different forces (0.4 N and 0.8 N) for the experiments in soaked conditions.

compensation based on this decreasing initial displacement could not be attempted. For this reason the first experimental point are not reliable and it was decided to cut them off thereby returning to the classical description of creep. This decision has however the consequence of inserting a source of error in the fitting procedure because it will be assumed that the force has been equal to the asymptotic value of the exponential model ever since the beginning of the experiment. Of course only the experimental points after the stabilization of the force at sample are actually processed. A second consequence is that the instantaneous elastic response cannot be realistic since at the time zero the real deformation is zero because the real force is still zero. The resulting values are presented in table 2 for the Zener model and in table 3 for the Burgers model.

As it was clear by the obtained results (see e.g. figure 5.2) both the models are good in this situation. In fact the fitting procedure converged in all the 11 experiments for both of them. In this work, however, the Burgers model will be preferred over the Zener model. From a quantitative standpoint it is more accurate because the mean of the squared 2-norm of the residuals for the Burgers fit is 5.2e-05 while for the Zener fit it is 10.1e-05. As for its physical correspondence the former is able to show two different stages with an exponential transient and a linear steady state while the latter does not have this long term behaviour. On the other hand this infinite strain at infinite time under finite stress is not realistic. Care must be taken when defining the time boundaries for the validity of the model. If very long times were of interest, though, corrective terms could be added, for example an exponential decay

of the isolated dashpot of the Burgers model.

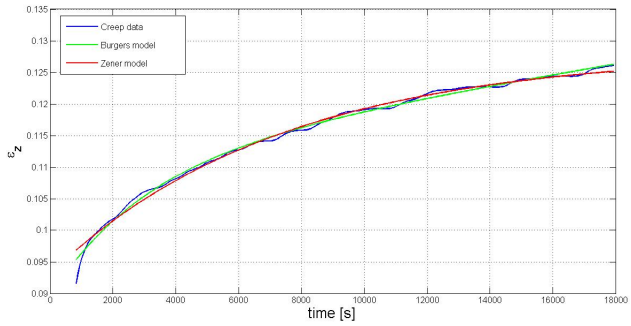

(a)

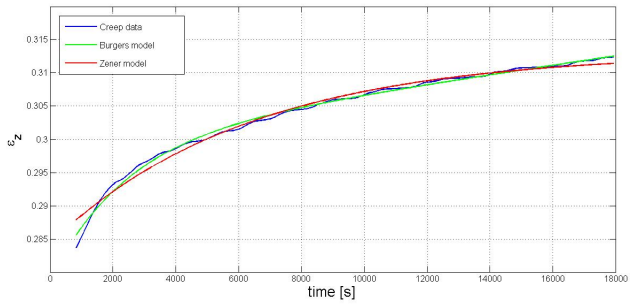

(b)

Figure 5.2: Result of the fitting procedure for the axial vertical strain ϵ_z over time for the fabric in a) dry conditions and constant force of 0.2 N and b) soaked conditions and constant force of 0.8 N. Both the considered viscoelastic models are effective in following the experimental data.

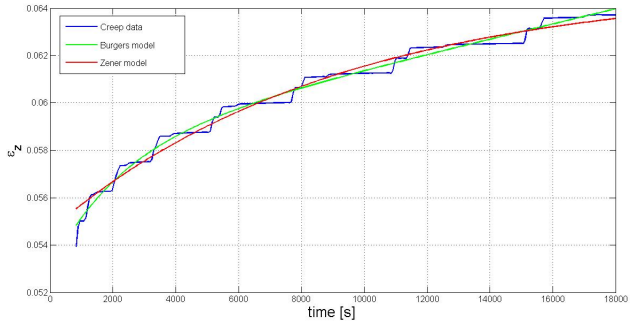

(a)

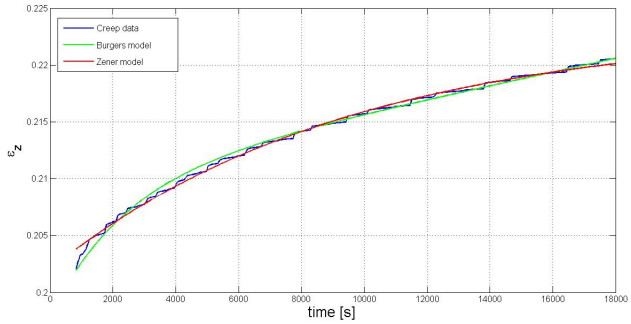

(b)

Figure 5.3: Result of the fitting procedure for the PLA fabric in a) dry conditions and constant force of 0.2 N and b) soaked conditions and constant force of 0.8 N. When the force is too small the behaviour is markedly step like.

	Fabric		
F [N]	Dry conditions		
	k_1 [kPa]	k_2 [kPa]	c_1 [kPa·s]
0.2	5.72	15.1	3.04e4
0.4	-	-	-
0.8	3.26	23.0	1.98e4
	Soaked conditions		
0.2	11.1	32.1	5.15e4
0.4	5.82	30.8	2.72e4
0.8	3.46	34.1	1.99e4

	Scaffold		
F [N]	Dry conditions		
	k_1 [kPa]	k_2 [kPa]	c_1 [kPa·s]
0.2	8.32	43.8	6.32e4
0.4	2.11	38.8	1.30e4
0.8	2.50	56.7	1.29e4
	Soaked conditions		
0.2	8.07	39.2	8.67e4
0.4	4.84	33.7	5.83e4
0.8	6.88	65.2	5.91e4

Table 2: Zener model parameters from creep experiments. The dry fabric was not tested under a force of 0.4 N.

	Fabric			
F [N]	Dry conditions			
	k_1 [kPa]	c_1[kPa·s]	k_2 [kPa]	c_2 [kPa·s]
0.2	90.2	2.85e5	21.7	2.29e6
0.4	-	-	-	
0.8	293	8.43e5	26.7	7.45e6
	Soaked conditions			
0.2	140	2.21e5	50.4	4.31e6
0.4	242	5.25e5	38.2	8.12e6
0.8	507	12.2e5	38.3	15.1e6

	Scaffold			
F [N]	Dry conditions			
	k_1 [kPa]	c_1 [kPa·s]	k_2 [kPa]	c_2 [kPa·s]
0.2	540	1.24e6	53.8	8.94e6
0.4	1050	2.22e6	41.4	27.3e6
0.8	1320	2.84e6	60.1	79.3e6
	Soaked conditions			
0.2	685	1.21e6	48.8	6.82e6
0.4	762	1.81e6	39.2	9.25e6
0.8	1220	2.88e6	73.5	24.2e6

Table 3: Burgers model parameters from creep experiments. The dry fabric was not tested under a force of 0.4 N.

As already discussed, viscoelastic materials can be analyzed scanning their response to sinusoidal loadings at different frequencies. If viscoelastic models are used for their description this is also a way to determine the parameters of the model. Since the response to cyclic prolonged loads is of interest in cartilage related researches, one of the possibilities for the experimental characterization of polymeric scaffolds, as well as for the computer simulations, could be in the frequency domain. Before doing so, though, the plot of E^* against $\log \omega$ can also be drawn on the basis of the parameters deriving from the fitting of the creep curves. Both the analyzed materials showed values for the viscous parameters much higher than those of the elastic parameters. By looking at figures 3.2 and 3.4 it is clear that materials well described by simple models having two elastic parameters present a transition between a lower stiffness in the low frequency region and a higher stiffness the high frequency region. This is visible by the two plateaus in the storage modulus. At the same frequency relative to this transition there is also the maximum value for the loss modulus. In the Burgers model there are two critical regions because at the lowest frequencies the model starts to move toward a purely viscous flow without any elastic stiffness. By the way, increasing values for the viscous parameters cause the critical frequencies to move toward lower values (for example in the Zener model frequency and dashpot constants appear always together, $c_1\omega$ and $c_1^2\omega^2$). By using a typical set of values from one of the creep experiments (where the elastic parameters range over few to tens of kPa (Zener model) or tens to hundreds of kPa (Burgers model) while the viscous parameter range over tens of thousands of kPa·s (Zener model) or millions of kPa·s (Burgers model)) it can be shown how it would be necessary to move to extremely low frequencies in order to capture the transitional regions for this systems. The typical frequency for human activities such as walking,

running, going up or down the stairs and so on is around 1 Hz. Here is presented the frequency response over the range from 10^{-3} to 10^{3} Hz as it can be estimated from the creep data. From this it is safe to say that the normal working range would be inside the high frequencies domain, with no frequency dependence whatsoever. Something starts changing going under 0.01 Hz, but it is also worth noting on the vertical axis the actual impact of this variations.

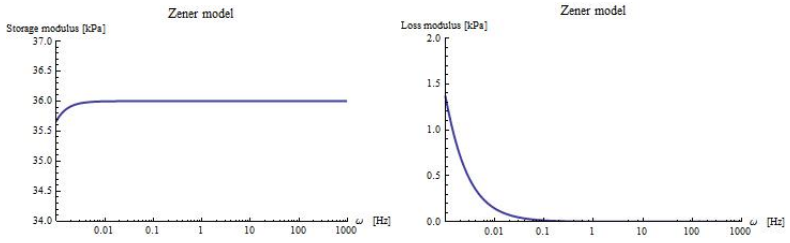

(a) Storage modulus

(b) Loss modulus

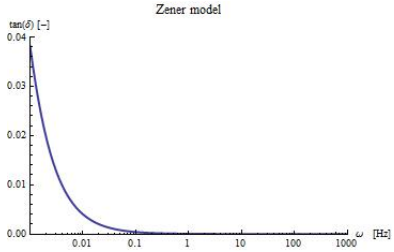

(c) tan(δ)

Figure 5.4: Frequency response for the soaked sample on the basis of parameters deriving from the fitting of a creep experiment with the Zener model.

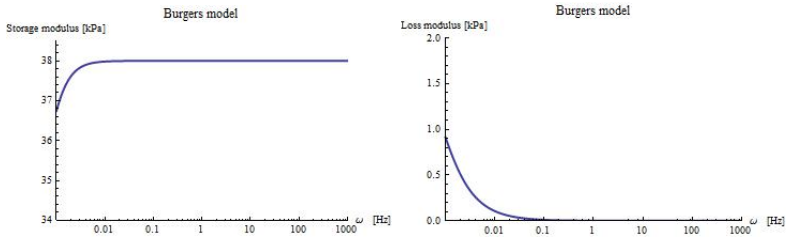

(a) Storage modulus (b) Loss modulus

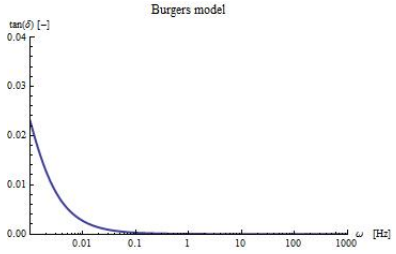

(c) tan(δ)

Figure 5.5: Frequency response for the soaked sample on the basis of parameters deriving from the fitting of a creep experiment with the Burgers model.

5.2 Materials characterization

From the creep experiments it is clear that the model parameters depend on the applied constant stress. It also appears that for both the viscosity constants and for the Kelvin spring the trend is linear with the applied stress (figure 5.6). So these three parameters obey to: $y^* = y^{ref} + m\,(\sigma_0 - \sigma_{ref})$, taking one of the stresses as the reference. The Maxwell spring does not show a clear dependence but its variations are quite small. Therefore its value will be assumed as the simple average between the three experimental values.

$$k_1^* = k_1^{ref} + m_{k_1}\,(\sigma_0 - \sigma_{ref}) \tag{5.1}$$

$$c_1^* = c_1^{ref} + m_{c_1}\,(\sigma_0 - \sigma_{ref}) \tag{5.2}$$

$$k_2^* = k_2^{ave} \tag{5.3}$$

$$c_2^* = c_2^{ref} + m_{c_2}\,(\sigma_0 - \sigma_{ref}) \tag{5.4}$$

Where the values come from fitting creep experiments. For the fabric $\sigma_{ref} = 5.41$ kPa.

	k_1 [kPa]	c_1 [kPa·s]	k_2 [kPa]	c_2 [kPa·s]
y_{ref}	252	5.35e+05	42.3	7.91e+06
m	47.7	1.28e+05	/	1.38e+06

For the scaffold $\sigma_{ref} = 5.37$ kPa.

	k_1 [kPa]	c_1 [kPa·s]	k_2 [kPa]	c_2 [kPa·s]
y_{ref}	810	1.80e+06	53.8	1.00e+07
m	45.4	1.25e+05	/	1.52e+06

Therefore the following expressions are given for the creep function and for the creep modulus, valid in the investigated range of 2 to 10 kPa.

$$\epsilon(t) = \frac{\sigma_0(1 - e^{-\frac{t}{\tau}})}{k_1^{ref} + m_{k_1}(\sigma_0 - \sigma_{ref})} + \frac{\sigma_0}{k_2^{ave}} + \frac{\sigma_0 t}{c_2^{ref} + m_{c_2}(\sigma_0 - \sigma_{ref})} \tag{5.5}$$

$$E(t) = \left(\frac{1 - e^{-\frac{t}{\tau}}}{k_1^{ref} + m_{k_1}(\sigma_0 - \sigma_{ref})} + \frac{t}{k_2^{ave}} + \frac{1}{c_2^{ref} + m_{c_2}(\sigma_0 - \sigma_{ref})} \right)^{-1} \tag{5.6}$$

Where the relaxation time is

$$\tau = \frac{c_1^{ref} + m_{c_1}(\sigma_0 - \sigma_{ref})}{k_1^{ref} + m_{k_1}(\sigma_0 - \sigma_{ref})} \tag{5.7}$$

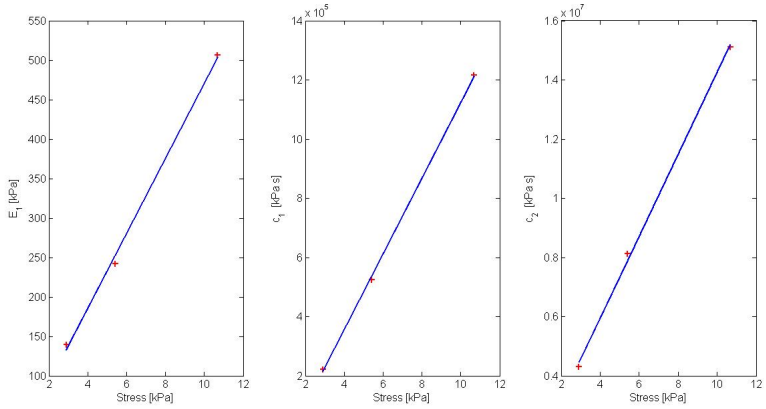

(a) Fabric, soaked.

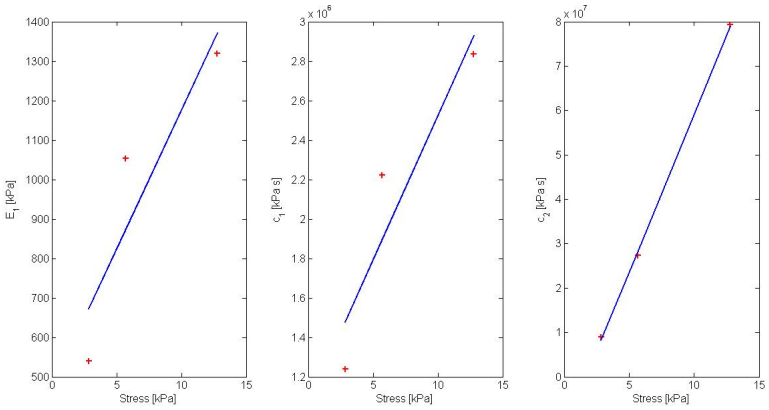

(b) Scaffold, dry.

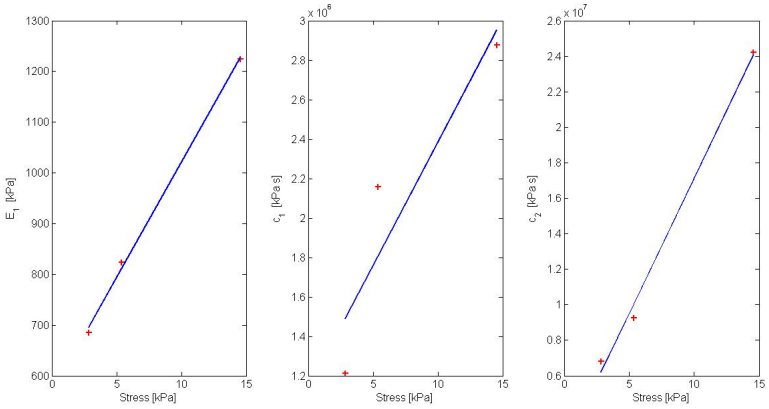

(c) Scaffold, soaked.

Figure 5.6: Linear trend in the viscoelastic parameters of the Burgers model for both the materials and in both dry and soaked experiments.

5.3 Setup of the finite element simulation

The FEM analysis are basically composed of the following steps:

- Definition of the application mode, i.e. physics or multiphysics of the problem.
- Creation of the geometry.
- Definition of the subdomain parameters.
- Definition of the boundary conditions.
- Initialization of the mesh.
- Definition of the solver parameters.
- Solution and postprocessing.
- Eventual analysis of convergence.

This section presents the results of the simulations carried out using two different application modes to deal with the same experiment, i.e. the unconfined creep test. The simplest case is to perform a transient analysis within the structural mechanics section. In this case it is possible to give the time dependent creep modulus and follow the displacement that is caused by the applied constant force. In a second moment also a poroelastic analysis will be done. This analysis combines a transient stress-strain section and a fluid mechanics section in a multiphysics problem. The setup of the simulation is different.

5.3.1 Application mode

Viscoelasticity intrinsically contain the time variable inside the definition of the material properties. The structural mechanics transient analysis is the correct one if the time evolution of the system is of interest. The dependent variable that is solved for is the displacement field $\mathbf{u}(\mathbf{r})$. From this quantity the strain is derived by definition of strain itself while the stress is calculated using the material properties. This analysis is of course nonlinear, since it is considered that the evolution of the body can depend on the whole history of the simulation. It will be important to keep the number of elements as low as possible and for this reason, as it will be repeated later, symmetry is exploited.

Poromechanics on the other hand is the science that studies the coupling between a solid matrix and the presence of a fluid inside its porosity, resulting in the response

of the global material that has both a mechanical part, with the matrix displacement field $\mathbf{u}(\mathbf{r})$, stress tensor $\boldsymbol{\sigma}(\mathbf{r})$ and strain tensor $\boldsymbol{\epsilon}(\mathbf{r})$, and a fluid dynamic part characterized by a pressure field $p(\mathbf{r})$ and velocity field $\mathbf{v}(\mathbf{r})$. This means that this is a multiphysics problem, implemented in Comsol in the Earth Science Module with the assumption of linear poroelasticity. The dependent variables which the program solves for are the matrix displacement and the fluid pressure. Stress and strain are then derived by means of the definition of strain and of the constitutive equations while the velocity field derives by Darcy's law through the pressure gradient.
Whenever possible in computer simulations it is very important to make use of symmetries, if present, because the solving time depends on the volume (or area depending on the dimensionality) of the model, i.e. on the *number* of the elements. For example in a 2D plane model having a symmetry means that only half of the elements are required. The exploitation of this fact means that either the same mesh can bring to the solution in half of the time or that with the same computational time it can be refined up to double its elements. Of course this aspects become more and more important if nonlinearities are present in the problem, as it happens in this work. It is worth noting that the same symmetry characteristics must be present both in the geometry and in the loading conditions. This was the case, and consequently all the analysis is *2D axial symmetric* and all the quantities are expressed as functions of the cylindrical coordinates (r, ϕ, z), of which only on r and z there can be explicit dependence.

5.3.2 Geometry

The geometry of the scaffolds is simply cylindrical. Thus for drawing the model all what is needed is a rectangle, having the height of the fabric and its radius as horizontal side, placed with one of the vertical sides in correspondence of the symmetry axis at $r = 0$.
The actual dimensions are 3 mm for the height and 5 mm for the radius.

5.3.3 Subdomain parameters

The structural mechanics model requires as an input the materials properties for each subdomain, or analyzed volume. They are mainly the elastic constants E and ν, the thermal constants and, in case, the body load due to gravity. In a viscoelastic analysis the only two that are of interest are the elastic ones. In this case it was required a careful fitting of the whole creep experiment in order to have consistent results. The time variable t can enter the definition of all the material properties. The solver will take care to update the numerical value at every timestep.

The poroelastic model has two different environments, axial symmetry stress-strain for the solid matrix and Darcy's law for the fluid. Both the environments require the definition of their parameters.
For the matrix they are the elastic modulus and the Poisson's coefficient. The elastic modulus is here considered to be the drained modulus [15], that is the one that the material has when the fluid can exit the porosity keeping a constant pressure (in perfect drained conditions there is a fluid flow and the fluid pressure is constant, in perfect undrained conditions the fluid cannot move and therefore if the body is compressed the fluid pressure will rise).
It is important to note that even if the software implements linear elasticity the solver works in a time dependent mode (theory explains that coupling with fluid motion makes the problem's type to become transient also in the stress-strain component). For this reason it is possible to include a time-dependency for the elastic properties simply in their initial definition. The software in this kind of problems already defines a time variable, with actual physical meaning (also in nonlinear elasto-plastic structural mechanics analysis there is a time variable, but in that case it is only a fictitious time). At the beginning of each time step the elastic modulus can be automatically updated to a different value. This enables to include for example linear viscoelastic features for the matrix properties, as it has been done in previous studies on cartilage [13]. However, the underlying theory remains of linear elasticity, therefore phenomena such as hysteresis or phase shifts in dynamic loading cannot be described. Also a body force is present, because of the weight of the infiltrating fluid. Given the size of the sample and the comparison with the applied external forces it is negligible, however it has been left.
The fluid dynamic part requires the parameters of Darcy's law and the volume fraction and compressibility for fluid and solid. Also in this case it is possible to update the values at every time step and it is done for the matrix compressibility and for the intrinsic permeability.

5.3.4 Boundary conditions

The boundary conditions, just like the subdomain settings, are to be defined both in the stress-strain and, if present, in the fluid side. For the mechanical part the these are the standard load and constraints definitions. Clearly they change according to the goal of the simulation, but in any case in free compression tests the constraints of axial symmetry on one of the vertical side, any constraint on the other and roller on the bottom side will be present. What differentiates the various cases is the settings on the top side. When modelling creep the constraint is free and there is an applied,

distributed constant load (in Pa), when modelling stress relaxation the distributed load is zero and the displacement of the top side is prescribed and constant, when modelling the dynamic response the way is twofold, either the displacement is set as sinusoidally varying over time (leaving as dependent variable the corresponding load that the moveable head has to apply, which is the integral of the stress induced in the surface of the material), i.e. displacement controlled tests, or the load is harmonic and the dependent variable is the displacement of the sample surface, i.e. load controlled tests.

5.3.5 Mesh

Given the simplicity of geometry and load conditions the definition of the mesh is not at all problematic in this case. Normally the cases in which it is necessary to be careful are when there are complex geometries or stress intensification regions such as angles or section changes, or when there are loads applied in small regions, such as contacts with sharp-cornered objects (that may be the case of constraints or of applied forces, for example in the simulation of indentations). In this case the force is applied on the whole sample (top) surface, and the reaction is applied on the entire (bottom) surface. The geometry is a rectangle, and so the automatic free mesh is created by the software without imposed settings. 2D triangular elements are used for the free mesh (figure 5.7).

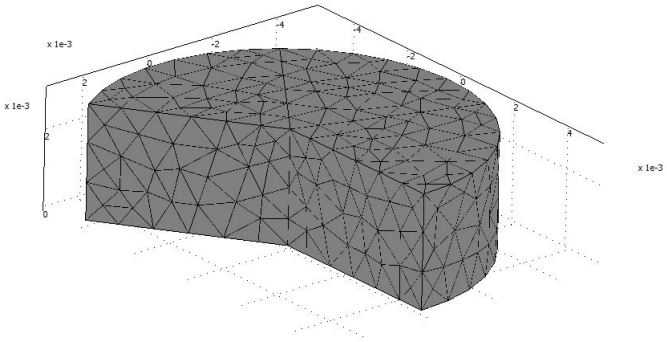

Figure 5.7: Visualization of the mesh. A 3D picture is presented but this is only a graphical revolution of what is actually a 2D mesh.

5.3.6 Solver parameters

This is in both the cases a nonlinear transient analysis. Therefore the solver is set on the time dependent mode and the time interval where the solution is calculated must be specified, as well as the time step Δt. The software starts at time $t_0 = 0$ with the given initial boundary conditions and solves for the initial values of stress,

strain and fluid pressure. Then updates all the parameters at time $t_0 + \Delta t$ and finds the new system configuration starting from the previous one, and this is repeated N times till the final time $t_f = t_0 + N\Delta t$ is reached. Like all the numerically solved problems, the goal is to converge to a certain unknown solution starting from a known initial condition. The solution is said to be found if some exit condition is reached, that is when it in stable over subsequent iterations. There is the possibility that the solver does not find this convergence because the time step is too wide, in this case a refinement is required, even if of course this means increasing the computational time.
in dynamic analysis there are also other issues related to the time dependent nature of the applied load. It is straightforward that the time steps should be short when compared to the period of the oscillations, otherwise there are in simulations the same problems associated with aliasing that are in the sampling of the real experiments.

5.4 Viscoelastic analysis

The first result that is expected from this analysis is that it is able to follow the experimental creep. The goodness of the creep modulus was already checked during the fitting procedure so this reduces to confirm that if the boundary conditions are well posed the software reaches the solution that is already expected. In figure 5.8 the FEM strain is shown to approach the strain calculated from the experiment. As an example the experiment om the fabric in water with a creeping force of 0.4 N was chosen.
Another thing that was noted is that the transient mechanical analysis does not see changes in the Poisson's ratio neither for the vertical strain nor for the Von Mises stress (figure 5.9). In the poroelastic model, as it will shown, this is no longer true. This is not surprising since the volumetric strain, which is affected by this elastic constant, controls the amount of fluid that leaves the solid and therefore has eventually to play a role.

5.5 Poroelastic analysis

In this case the big number of the parameters that are required for reaching a solution makes the things a little bit harder. Once again some of the information can be extracted from the data. However using the same time dependent modulus would not be correct because it already includes the effects of the presence of the fluid, which is what is now added with the multiphysics approach. Moreover, also

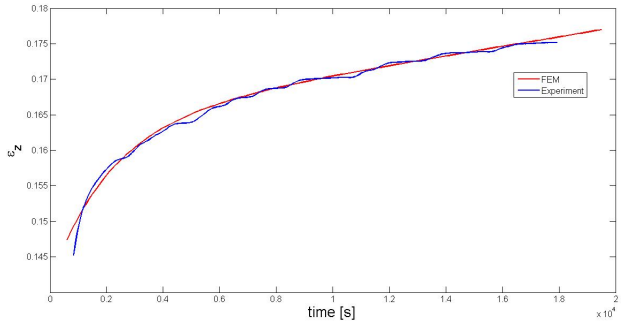

Figure 5.8: Time evolution of the vertical strain ϵ_z during the creep experiment at 0.4 N. The viscoelastic FEM solution is well capable of describing the experiment.

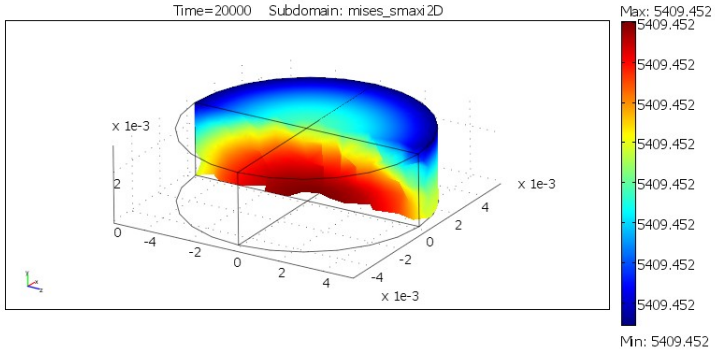

Figure 5.9: 3D revolution of the visualization of the Von Mises stress at the end of the simulation. By looking at the colour legend it is clear that all the volume is equally stressed.

the Poisson's coefficient is not known, since the radial displacement was not measured. A second important value of which is required to give an estimation is the matrix permeability, for the definition of which a strain dependent formulation is used (equation 3.76), based on the simple model previously explained. These two issues, of the elastic and permeability values, will be addressed together.

5.5.1 Creep simulation

The starting observation is that when running a simple creep simulation at constant elastic modulus the system reaches the asymptotic strain after what is called consolidation time, a property of the poroelastic media dependent precisely on the

parameters at hand [16].

$$\tau = \frac{\mu a^2}{Ek} \frac{(1+\nu)(1-2\nu)}{(1-\nu)} \tag{5.8}$$

Where a is a typical length (the disk diameter in this case). A qualitative trend for τ is sketched in figure 5.10.

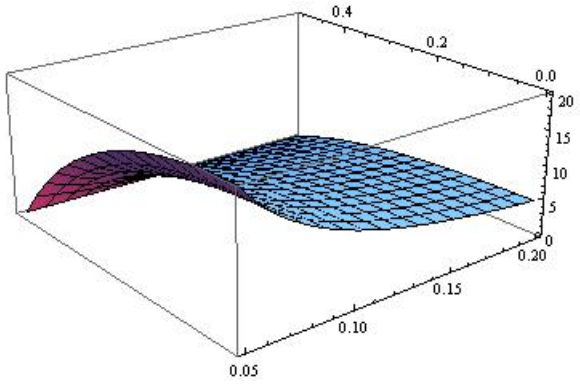

Figure 5.10: Plot for the trend of the consolidation time when the permeability and the Poisson's ratio are chosen as parametric variables. Arbitrary units.

The idea is that the missing values among the 5 entering the definition of this characteristic time can be estimated by running several simulations parametrical in these unknowns (see figure 5.11 and 5.12 for an example of the parametric analysis that were performed in this thesis work). This was possible because also by the look at the creep strain this separation into initial and long-term behaviour can be spotted.

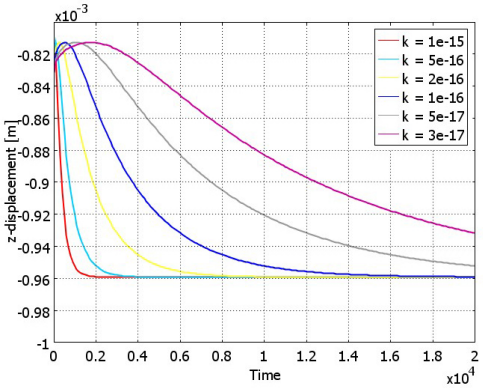

Figure 5.11: Example of parametric analysis of the vertical displacement of the upper surface with decreasing matrix permeability. The values are in m^2.

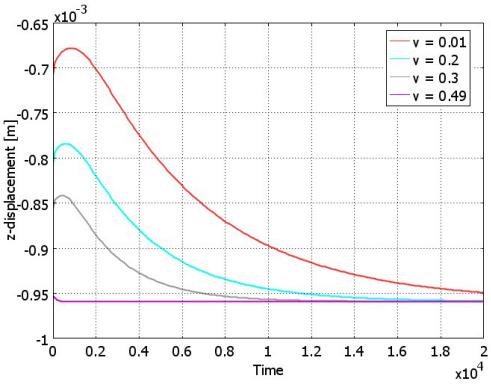

Figure 5.12: Example of parametric analysis of the vertical displacement of the upper surface with different Poisson's ratii.

The second observation is that in the same preliminary simulations was noted that the fluid pressure reaches a constant value after this consolidation time. This,

combined with the fact that the implementation of poroelasticity in Comsol uses the drained modulus, which is present exactly in this condition, suggested that for the value of the elastic modulus just the long term response was required.
Therefore the first usage of the finite elements simulations was to get as estimation for the permeability and for the Poisson's ratio of the scaffolds, provided that their elastic moduli had already been extracted by the creep data and that the dynamic viscosity for water had been set to the canonical value of 0.001 Pa·s.
The numerical values are presented in table 4. For these values no experimental proof was available. k should be a property of the structure. However a certain variability is observed, and the scaffold seems to be more permeable when the imposed pressure gradient is smaller.
Given the big deformations to which the samples were subjected, finally, the fact that the Poisson's constant is not a material property is not in contradiction with what already found, for example, as for the parameters of the viscoelastic models of the same experiments.

Creep force [N]	k [m^2]	ν [-]
0.2	5e-16	0.15
0.4	2e-16	0.30
0.8	4e-17	0.37

Table 4: Estimation by FE optimization of matrix permeability and Poisson's coefficient for the PLA fabric.

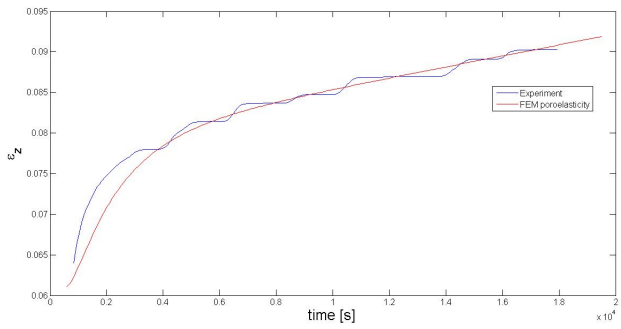

Figure 5.13: Image from the poroelastic simulation of the 0.2 N creep experiment showing the good agreement between model and measurements once that the parameters are parametrically fixed.

The FEM solution can now be used to look inside the material. In order secure the convergence the system is initialized in the undeformed configuration and the constant force is applied bt an exponential function. This is exactly what happens in the experiments and indeed the time constant for this function is taken from the analysis of the data and set to 185 s.

Firstly the attention is focused on the fluid related quantities pressure and velocity field. The pressure has to *rise* inside when the pushrod applies the force but it is interesting to note how after suddenly rising it *decreases* to reach asymptotically zero within what can be seen as the relaxation time of the poroelastic system. Figure 5.14 refers to the center of the sample during the experiment at 0.8 N. The shape of the pressure profile is reflected in the velocity field, which is proportional to its gradient. Also this field has the same feature of a sudden increase followed by a slightly less sloping decay, but everything happens in the very first part of the experiment. Figure 5.15 shows the plot of the surface integral of the velocity field over the vertical wall of the specimen, it is therefore the plot of the flow rate in m^3/s.

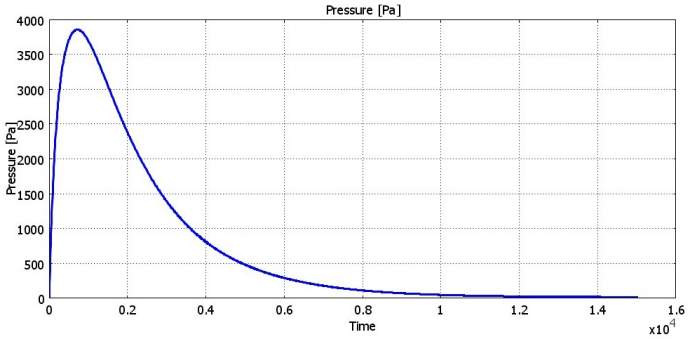

Figure 5.14: Fluid pressure at the center of the upper surface of the sample The applied external stress is 14.55 kPa thus the fluid reaches at maximum around 4 times lower a pressure. This maximum is reached after 750 s and the fluid pressure is less than one tenth of this maximum value after around 5500 s.

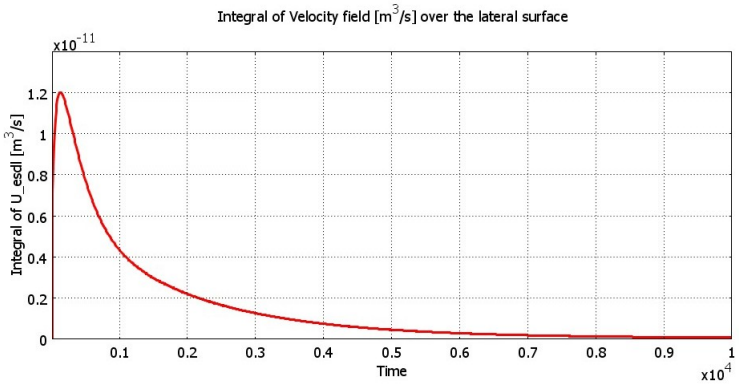

Figure 5.15: Flow rate through the open lateral boundary. The maximum is reached after 450 s.

The time evolution of the pressure and of its gradient were also plotted in the simulated subdomain, choosing significant time slices according to figure 5.14. It can be seen that only in the core of the sample the fluid pressure actually increases

whereas at the external surface it remains close to zero (figure 5.16). At the beginning the force is rising and the pressure is still zero. When the pushrod tries to compress the material the fluid inside sustains part of the pressure and the overall stiffness of the scaffold is in this moment higher. Due to the pressure gradient the water starts to exit the matrix and the pressure relaxes to zero. This ultimately results in a lowering also of the fluid rate.

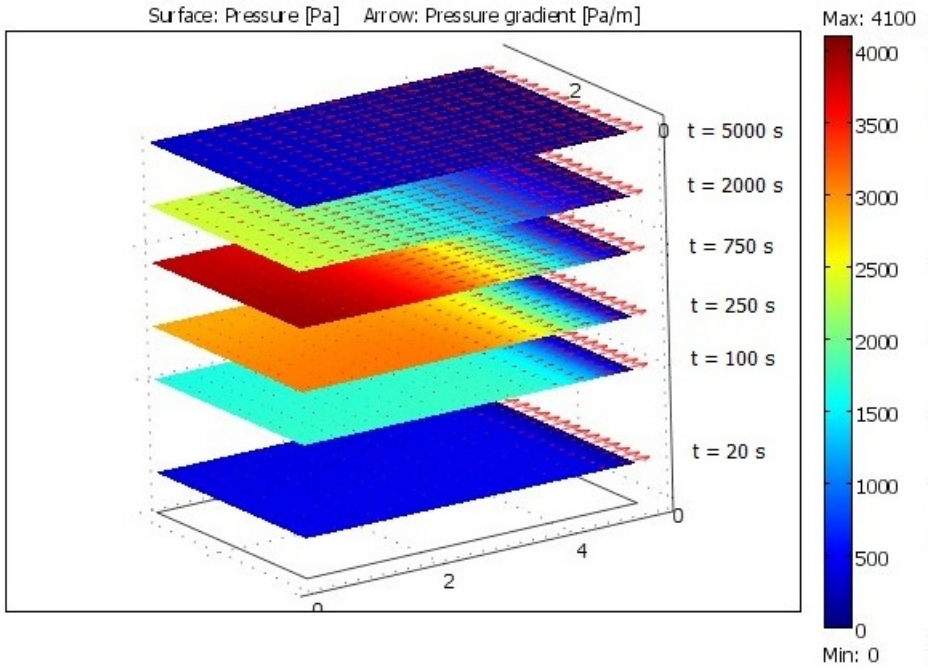

Figure 5.16: Spatial and temporal trend for the fluid pressure (colour map) and for the pressure gradient (arrow plot) for the creep experiment at 0.8 N. The single slice refers to one snapshot at the indicated time (the spacing is in a logarithmic scale) of the simulated box, i.e. half of a vertical section of the specimen. The arrow plot does not have a normalized scale.

Now, turning the attention to the matrix stress, it was noted that in this case the value is more or less *constant* after the moment when the force has reached the constant value. The deformation goes on since the fluid is going out of the matrix but the stress felt by the matrix itself does is not changed. This was also observed in the simulations implementing the creep time dependent modulus. In figure 5.17 the Von Mises stress is plotted on the sample section at the beginning (1000 s) and ending (15000 s) of the simulation. The stress is firstly nearly constant over all the geometry (variations of 4 % and 0.2 % respectively) and secondly very close to the applied 14.55 kPa. This means that the only important stress is the simple axial compression.

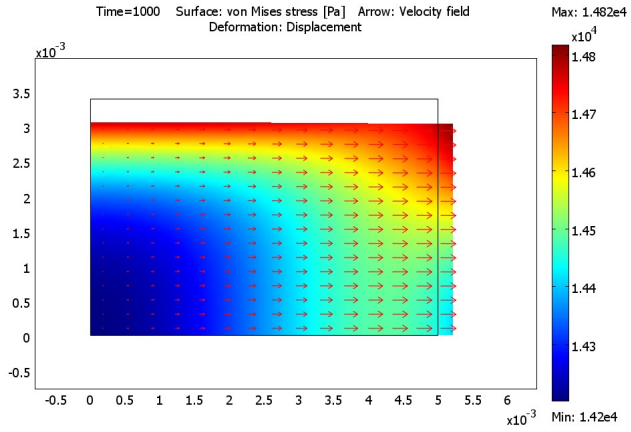

(a) t = 1000 s

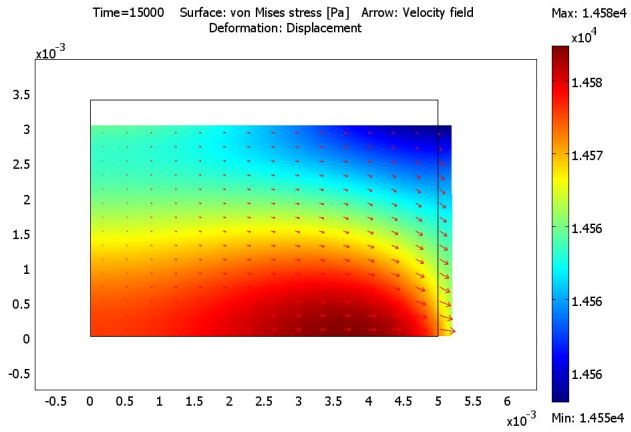

(b) t = 15000 s

Figure 5.17: Map of the Von mises stress inside the sample in the first (a) and final (b) part of the experiment. It should be noted as the colour scale runs over a narrow range of values, and also that the maximum absolute value decreases only by 2 % between a) and b).

5.5.2 Dynamic simulation

The modelling of the creep tests is important to complete the set of parameters. A more interesting situation is, however, the dynamic configuration. The former represents, for example, the action of standing, the latter may represent the walking. In order to test the scaffold in a condition as close as possible to its applications the dynamic simulation is performed using an harmonic solicitation at a physiological frequency of 1 Hz. It is in displacement control mode, so as not to have the superposition of dynamic strain and creep strain. This is a compression test, so the net force cannot ever change sign and in order to have harmonic oscillations a constant

mean negative value must be kept either for the force (if stress control) or for the displacement (if displacement control).
In order to set the amplitude of the oscillations, again, a physiological value was desired. From *in vivo* tests found in literature [22] on the cartilage deformation in the femorotibial compartment this value was set to 5 %, looking at the values of the patellar cartilage deformation during knee bending (5.9 %), walking (2.8 %) and running (5.0 %). Given the initial height of the samples, this means an amplitude of 70 μm. The elastic modulus was given by the Burgers creep modulus at the beginning of the (meaningful part of the) experiment, since in this case the material does not have time to relax. The parameters of the simulation are summarized in table 5.

Upper displacement [μm]:	$u_z = -75 - 70\sin(2\pi t)$		
Stress-strain environment		Fluid dynamics environment	
E [kPa]	71.8	n	80 %
ν [-]	0.37	χ^w [Pa^{-1}]	4.4e-10
		k [m^2]	4e-17
		μ [Pa·s]	0.001

Table 5: Set of parameters and imposed solicitation for the modelling of the dynamic response.

Analyzing the results of the simulation it appears immediately that the pressure distribution, and consequently the velocity field, the two most important variables as for the biological response of the scaffold, are basically *constant* throughout all the material, except for a strong border effect. In particular in the 80 % of the scaffold the discharge velocity remains below 10^{-8} m/s. Thus most of the volume experiences what goes under the name of undrained deformation. The pressure is of course changing over the time because of the imposed deformation, but it can be observed how it changes it the same way across almost all the scaffold. Therefore there the pressure gradient is zero.
It can also be observed that pressure and displacement are in phase (the maximum of the compression, i.e. the instant when u_z is more negative, correspond to the maximum in the fluid pressure, see figure 5.18). This is what is reasonable to expect and also presented in other early studies [18]. Snapshot of the postprocessing animation are presented in figure 5.19.

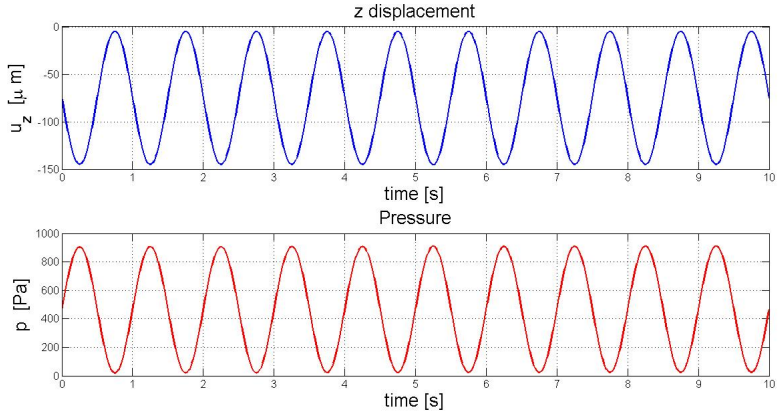

Figure 5.18: Pressure value at the center of the upper surface (blue line) resulting by the application of controlled displacement at a frequency of 1 Hz (red line). When the scaffold reaches the maximum compression the pressure inside reaches the maximum value, with to appreciable phase shift.

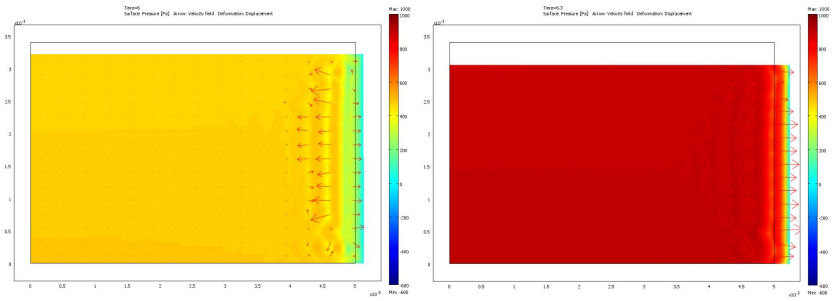

(a) Passage through the mean position.

(b) Maximum compression.

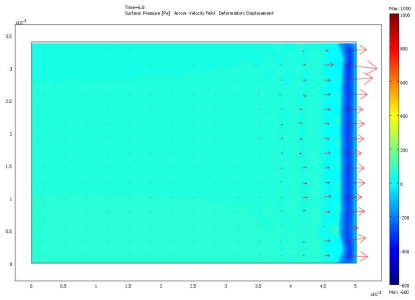

(c) Maximum decompression.

Figure 5.19: Surface plot of the dynamic response in displacement control, after 5 cycles put to reach a steady state. The period of the oscillation is 1 s.The colour scale refers to the fluid pressure while the arrows are representing the velocity field. The fluid pressure is not symmetric and for the major part of the volume it remains always positive even if for 50 % of the time the solicitation is such as to induce a depression inside the pores.

As already said, 1 Hz is a typical frequency of many human activities. However what would happen with much slower variations of the same applied displacement? For a comparison, the same situation has been modelled (i.e. keeping all the pa-

rameters as before) changing only the frequency of the sinusoidal imposed upper boundary condition from 1 s to 5000 s (around one and a half hour), representative for example of alternation between standing and sitting. If at 1 Hz it is clear that the fluid velocity has no time to follow the variation of the porosity that would bring to a sinusoidal turnover between entering and exiting the scaffold, this time this is what is reasonable to expect. The simulation showed that the fluid motion now regards most of the volume and there is a pressure gradient along the r coordinate (but not along the z coordinate). The inside of the structure is not anymore kept in a constant pressurized state but there is an alternation of positive and negative pressure symmetric with respect to the zero. Also the maximum value is affected and it decreases from around 0.94 kPa to 0.57 kPa. The graphical postprocessing of this simulation is presented in figure 5.20.

Thus there is a clear change in the fluid response with an almost absent actual motion under rapidly varying situations and completely harmonic velocity field if the same deformation happen in a longer timespan. What must be said, though, is that the absolute value of the velocity, and consequently the flow rate of the possibly nutrient and oxygen carrying fluid, is unchanged. This is because the volumetric deformation, ultimately the driving force for the flow to happen, is quite small.

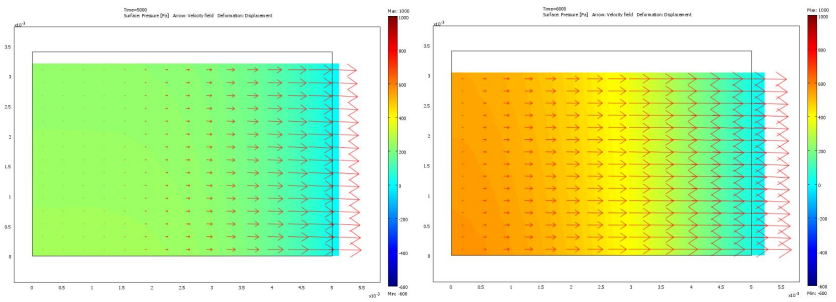

(a) Passage through the mean position.

(b) Maximum compression.

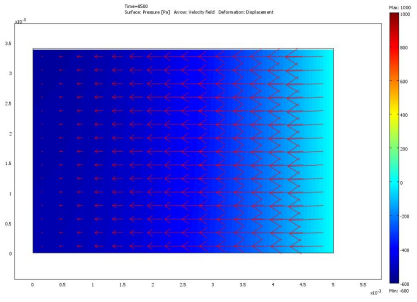

(c) Maximum decompression.

Figure 5.20: Surface plot same as that presented in figure 5.19 for the same scaffold and the same amplitude but with a period of 5000 s. The fluid pressure is now symmetric.

6 Conclusions and further developments

This work was born with the intention of modelling the behaviour of polymeric scaffold, with future applications in the cartilage repair, on the basis of data obtained by creep tests.

Two approaches were attempted. The first starts from the observation that the tissue of interest, i.e. the articular cartilage, has been extensively studied as a viscoelastic material. Following the same theory the fibrous scaffold could be described by viscoelastic models. Since it is important to maintain the description as simple as possible, for instance if future computational models will take advantage of this characterization, two simple models, known as Zener and Burgers models, were successfully tested.

The conclusion of this first part is that the theory of linear viscoelasticity is sufficient to well fit the creep data for both the models. The Burgers model was found to have a smaller value for the squared 2-norm of the residuals. Even if the single experiments, performed at different constant forces, follow linear viscoelasticity, the material cannot be considered as such since the fit parameters are not constants only of the material but changes for every experiment. For the Burgers model, though, three out of the four constants were interestingly found to be linearly dependent on the creep force, while the fourth remains approximately constant thereby allowing to identify an actual set of material parameters valid in the analyzed force interval.

The second approach used finite element simulations within the multiphysics environment of poroelasticity. The first step was to use the creep experiments to extract the parameters required by Biot's theory. The proposed method is to model the long term behaviour with a simple effective elastic modulus linearly time dependent and to estimate the remaining parameters by performing a parametric analysis. In a subsequent stage these results were used in a simple simulation of the dynamic response of the material subjected to a displacement controlled harmonic oscillation. The use of poroelasticity gives also the fluid dynamic inside the scaffold.

The result of the creep simulations is the estimation of the matrix permeability and the description of the fluid response under such a stimulation. It was observed that the stress inside the solid reaches rapidly the constant value imposed by the uniaxial compression while the fluid pressure first peaks, only in the central part of the sample, at a value of around one fourth of the applied stress and then decays to asymptotically reach zero. The time constant for the relaxation of the fluid pressure ranged from 2000 to 8000 seconds, increasing with increasing creep force. The result of the dynamic simulations is that for a physiological frequency of 1 Hz the inertia of the fluid inside the structure does not allow a significant motion. The pressure

is harmonic, in phase with the harmonic imposed displacement but remains always positive. It can be concluded that there would be no preferential zones for an eventual cell growth and that the physical stimuli, driving for example cell differentiation and genic expression, are the same over at least 90 % of the simulated volume. If the period of the oscillation is lowered to 5000 s a fluid velocity field is observed and involves also the internal part of the scaffold. The pressure is still harmonic but oscillates now around the zero.

Further developments must include an experimental study of the dynamic behaviour of these textiles to validate the predictions of the viscoelastic analysis. It would also be interesting to draw a parallelism between the viscoelastic and poroelastic description since both include a transition between different behaviours and both can be associated with a relaxation time. Another important issue of the present state of the FEM model is that in the used release of the software the analysis in frequency domain is not implemented and only the time dependent transient solver is available. It remains to check if this has been fixed in the newer versions. Finally, a last feature of the present experiments, and of the simulations as a consequence, is that they were carried out in unconfined compression mode. This is not the real situation since within the actual tissue the conditions would be certainly those of confined compression. However it is also true that if in the future these scaffolds will need a characterization as fast and simple as possible, the unconfined experiments would be preferable. The challenge then would be to develop a procedure, maybe precisely with the aid of the finite element simulations, which gives an estimation of, say, the confined bulk modulus starting from the value relative to unconfined tests.

References

[1] Verberne, Gabi, et al. "Techniques for assessment of wear between human cartilage surfaces." *Wear* 266.11 (2009): 1216-1223

[2] Mansour, J. M. "Biomechanics of cartilage." *Kinesiology: the mechanics and pathomechanics of human movement* (2003): 66-79.

[3] Nordin, Margareta, and Victor Hirsch Frankel, eds. *Basic biomechanics of the musculoskeletal system*. Lippincott Williams & Wilkins, 2012.

[4] Bachrach, Nathaniel M., Van C. Mow, and Farshid Guilak. "Incompressibility of the solid matrix of articular cartilage under high hydrostatic pressures." *Journal of biomechanics* 31.5 (1998): 445-451.

[5] Maurel, W., Wu, Y., Magnenat Thalmann, N., Thalmann, D. *Biomechanical models for soft tissue simulation*. Berlin: Springer-Verlag, 1998.

[6] Williams, David F. "On the mechanisms of biocompatibility." *Biomaterials* 29.20 (2008): 2941-2953.

[7] Capurso, M. *Lezioni di scienza delle costruzioni*. Pitagora editrice, 1998.

[8] Biot, Maurice A. "General theory of three-dimensional consolidation." *Journal of applied physics* 12.2 (1941): 155-164.

[9] E. Detournay, A.H.-D. Cheng, *Fundamentals of poroelasticity*, Chapter 5 in Comprehensive Rock Engineering: Principles, Practice and Projects, Vol. II, Analysis and Design Method, ed. C. Fairhurst, Pergamon Press, pp. 113-171, 1993.

[10] J. R. Rice, *Elasticity of Fluid-Infiltrated Porous Solids*, Harvard University. 1998.

[11] Selyakov, V. I., and V. V. Kadet. *Percolation models for transport in porous media*. Boston, London: Kluwer Academic Publishers, 1996.

[12] Hutton, David V., and Jianhua Wu. *Fundamentals of finite element analysis*. Vol. 1. New York: McGraw-Hill, 2004.

[13] DiSilvestro, Mark R., et al. "Biphasic poroviscoelastic simulation of the unconfined compression of articular cartilage: I-simultaneous prediction of reaction force and lateral displacement." *Journal of biomechanical engineering* 123.2 (2001): 191-197.

[14] Li, L. P., M. D. Buschmann, and A. Shirazi-Adl. "The asymmetry of transient response in compression versus release for cartilage in unconfined compression." *Journal of biomechanical engineering* 123.5 (2001): 519-522.

[15] Biot poroelasticity. Comsol application gallery. 2008.

[16] Naili, S., C. Oddou, and D. Geiger. "A method for the determination of mechanical parameters in a porous elastically deformable medium: applications to biological soft tissues." *International journal of solids and structures* 35.34 (1998): 4963-4979.

[17] Freutel, Maren, et al. "Finite element modeling of soft tissues: material models, tissue interaction and challenges." *Clinical Biomechanics* 29.4 (2014): 363-372.

[18] Manfredini, P., et al. "Poroelastic finite element analysis of a bone specimen under cyclic loading." *Journal of biomechanics* 32.2 (1999): 135-144.

[19] Li, LePing, J. T. M. Cheung, and W. Herzog. "Three-dimensional fibril-reinforced finite element model of articular cartilage." *Medical & biological engineering & computing* 47.6 (2009): 607-615.

[20] Laurent, Cedric P., et al. "Mechanical behaviour of a fibrous scaffold for ligament tissue engineering: Finite elements analysis vs. X-ray tomography imaging." *Journal of the mechanical behavior of biomedical materials* 40 (2014): 222-233.

[21] Netzsch DMA 242 E Artemis. Data sheet.

[22] Eckstein, F., et al. "In vivo cartilage deformation after different types of activity and its dependence on physical training status." *Annals of the rheumatic diseases* 64.2 (2005): 291-295.